Colloquium: Phononics: Manipulating heat flow with electronic analogs and beyond

Nianbei Li

NUS–Tongji Center for Phononics and Thermal Energy Science and Department of Physics, Tongji University, 200092 Shanghai, People's Republic of China, Department of Physics and Centre for Computational Science and Engineering, National University of Singapore, 117546 Singapore, and Max Planck Institute for the Physics of Complex Systems, Nöthnitzer Strasse 38, D-01187 Dresden, Germany

Jie Ren

Theoretical Division, Los Alamos National Laboratory, Los Alamos, New Mexico 87545, USA, Department of Physics and Centre for Computational Science and Engineering, National University of Singapore, 117546 Singapore, and NUS Graduate School for Integrative Sciences and Engineering, National University of Singapore, 117456 Singapore

Lei Wang

Department of Physics, Renmin University of China, Beijing 100872, People's Republic of China, and Department of Physics and Centre for Computational Science and Engineering, National University of Singapore, 117546 Singapore

Gang Zhang

Key Laboratory for the Physics and Chemistry of Nanodevices and Department of Electronics, Peking University, Beijing 100871, People's Republic of China, and Department of Physics and Centre for Computational Science and Engineering, National University of Singapore, 117546 Singapore

Peter Hänggi

Institut für Physik, Universität Augsburg, Universitätsstrasse 1, D-86135 Augsburg, Germany, Department of Physics and Centre for Computational Science and Engineering, National University of Singapore, 117546 Singapore, and Max Planck Institute for the Physics of Complex Systems, Nöthnitzer Strasse 38, D-01187 Dresden, Germany

Baowen Li*

NUS–Tongji Center for Phononics and Thermal Energy Science and Department of Physics, Tongji University, 200092 Shanghai, People's Republic of China, Department of Physics and Centre for Computational Science and Engineering, National University of Singapore, 117546 Singapore, and NUS Graduate School for Integrative Sciences and Engineering, National University of Singapore, 117456 Singapore

(published 17 July 2012)

The form of energy termed heat that typically derives from lattice vibrations, i.e., phonons, is usually considered as waste energy and, moreover, deleterious to information processing. However, in this Colloquium, an attempt is made to rebut this common view: By use of tailored models it is demonstrated that phonons can be manipulated similarly to electrons and photons, thus enabling controlled heat transport. Moreover, it is explained that phonons can be put to beneficial use to carry and process information. In the first part ways are presented to control heat transport and to process information for physical systems which are driven by a temperature bias. In particular, a toolkit of familiar electronic analogs for use of phononics is put forward, i.e., phononic devices are described which act as thermal diodes, thermal transistors, thermal logic gates, and thermal memories. These concepts are then put to work to transport, control, and rectify heat in physically realistic nanosystems by devising practical designs of hybrid nanostructures that permit the operation of functional phononic devices; the first experimental realizations are also reported. Next, richer possibilities to manipulate heat flow by use of time-varying thermal bath temperatures or various other external fields

*phononics@tongji.edu.cn

are discussed. These give rise to many intriguing phononic nonequilibrium phenomena such as, for example, the directed shuttling of heat, geometrical phase-induced heat pumping, or the phonon Hall effect, which may all find their way into operation with electronic analogs.

DOI: 10.1103/RevModPhys.84.1045 PACS numbers: 44.10.+i, 05.45.−a, 05.60.−k, 05.70.Ln

CONTENTS

I. INTRODUCTION

When it comes to the task of transferring energy, nature has at its disposal tools such as electromagnetic radiation, conduction by electricity, and also heat. The latter two tools play a dominant role from a technological viewpoint. The conduction of heat and electric conduction are two fundamental energy transport mechanisms of comparable importance, although they have never been treated equally in science. Modern information processing rests on microelectronics, which after the invention of the electronic solid-state transistor (Bardeen and Brattain, 1948), and other related devices, sparked off an unparalleled technological development, the state of the art being electric integrated circuitry. Without any doubt, this technology markedly changed many aspects of our daily life. Unfortunately, a similar technology which builds on electronic analogs via the constructive use of heat flow has not yet been realized by mankind, although attempts have been made repeatedly. In everyday life, however, signals encoded by heat prevail over those by electricity. Therefore, the potential of using heat control may result in an even more abundant and unforseen wealth of applications. It is legitimate then to ask whether phononics, i.e., the counterpart technology of electronics, presents only a dream.

Admittedly, it indeed is substantially more difficult to control *a priori* the flow of heat in a solid than it is to control the flow of electrons. This is because, unlike electrons, the carriers of heat, the phonons, are quasiparticles in the form of energy bundles that possess neither a bare mass nor a bare charge. Although isolated phonons do not influence each other, interactions involving phonons become of importance in the presence of condensed phases. Some examples that come to mind are phonon polaritons, i.e., the interaction of optical phonons with infrared photons, the generic phonon-electron interactions occurring in metals and semimetals, phonon-spin interactions, or phonon-phonon interactions in the presence of nonlinearity. Therefore, heat flow features aspects that in many ways are distinct from those of charge and matter flow. Nonetheless, there occur in condensed phases many interesting cross interplays as are encoded in the reciprocal relations of the Onsager form for mass, heat, and charge flow, of which thermoelectricity (Callen, 1960; Dubi and Di Ventra, 2011) or thermophoresis, i.e., the Soret versus its reciprocal Dufour effect (Callen, 1960), are typical exemplars. Therefore, capitalizing on the rich physical diversities involving phonon transport as obtained with recent successes in nanotechnology may open the door to turning phononics from a dream into a reality.

In this Colloquium we focus on two fundamental issues of phononics, i.e., the manipulation of heat energy flow on the nanoscale and the objective of processing information by utilizing phonons. More precisely, we investigate the possibilities of devising elementary building blocks for using phononics; namely, we study the conceptual realization and possible operation of a thermal diode which rectifies heat current, a thermal transistor that is capable of switching and amplifying heat flow, and last but not least a thermal memory device.

The objective of controlling heat flow on the nanoscale necessarily rests on the microscopic laws that govern heat conduction, stability aspects, or thermometric issues. For these latter themes the literature already provides us with several comprehensive reviews and features. For heat flow and/or related thermoelectric phenomena on the microscale, nanoscale, and molecular scale see the treatises by Lepri, Livi, and Politi (2003), Casati (2005), Li *et al.* (2005), Galperin, Ratner, and Nitzan (2007), Dhar (2008), Zhang and Li (2010), Pop (2010), and also recently by Dubi and Di Ventra (2011). We further demarcate our presentation from the subjects of refrigeration on mesoscopic scales and thermometry (Giazotto *et al.*, 2006). As our title suggests, we also do not address *per se* in greater detail the issue of the conventional way of manipulating heat flow upon changing the thermal conductivity by means of various phonon scattering mechanisms in nanostructures and heterostructures (Zimen, 2001; Chen, 2005). For compelling recent developments and

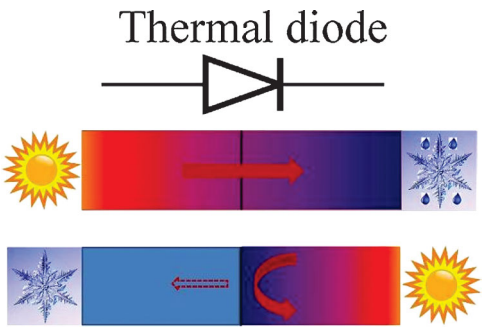

FIG. 1 (color). Sketch of the *modus operandi* of a thermal diode. When the left end of the diode is at a higher temperature as compared to its right counterpart, heat is allowed to flow almost freely. In contrast, when the right end is made hotter than the left,the transduction of heat becomes strongly diminished.

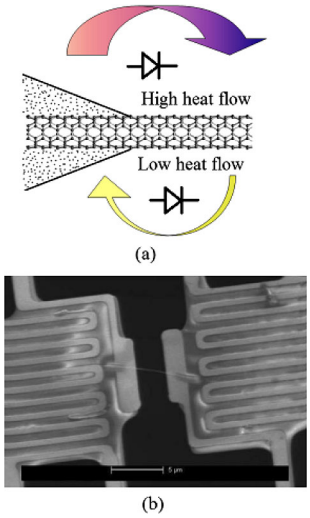

FIG. 2 (color online). Concept and experimental setup of a nanoscale thermal diode. An asymmetric nanotube is placed over two electrodes with one serving as a heater. For further details on the experimental procedures and the experimental findings see the experiment by Chang *et al.* (2006) and the detailed discussion in Sec. III. Adapted from Chang *et al.*, 2006.

advances in this last area see the recent surveys by Balandin (2005) and Balandin, Pokatilov, and Nika (2007), together with the original literature cited therein.

In this spirit, a primary building block for phononics is a setup that rectifies heat flow, i.e., a thermal rectifier or diode. Such a device acts as a thermal conductor if a positive thermal bias is applied, while in the opposite case of a negative thermal bias it exhibits poor thermal conduction, thus effectively acting as a thermal insulator, and possibly also vice versa. The concept of such a thermal diode is sketched in Fig. 1.

The concept of the thermal diode involves, just as in its electronic counterpart, the presence of a symmetry-breaking mechanism. This symmetry breaking is most conveniently realized by merging two materials exhibiting different heat transport characteristics. Historically, Starr (1936) built a junction composed of a metallic copper part joined with the cuprous oxide phase, thus proving the working principle of rectifying heat in such a structure. Starr's thermal rectifier is physically based on an asymmetric electron-phonon interaction occurring in the interface of the two dissimilar materials. There exist many such macroscopic rectifiers which function via the difference of the response of two materials due to temperature bias and/or other externally applied control fields such as strain, etc. (Roberts and Walker, 2011).

The focus of this Colloquium is on a thermal rectification scenario that is induced by phonon transport occurring on the nanoscale. The concept of such a thermal rectifier for heat was put forward by Terraneo, Peyrard, and Casati (2002). They proposed to use a three-segment structure composed of different nonlinear lattice segments. The underlying physical mechanism relies on the resonance phenomenon in the temperature-dependent power spectrum versus frequency as a result of the nonlinear lattice dynamics. Subsequently, it was shown that a modified two-segment setup (Li, Wang, and Casati, 2004, 2005) yields considerably improved rectification characteristics as compared to the original three-segment setup (Terraneo, Peyrard, and Casati, 2002). These pioneering works in turn ignited a flurry of activities, manifesting different advantageous features and characteristics. The theoretical and numerical efforts culminated in the first experimental validation of such a thermal rectifier in 2006: The device itself is based on an asymmetric nanotube structure (Chang *et al.*, 2006). The concept of this latter thermal diode together with its explicit experimental setup is depicted in Fig. 2.

The thermal diode presents an important first step toward phononics. For performing logic operations and useful circuitry, however, additional control mechanisms for heat are required. These comprise the tasks of devising (i) the thermal analog of an electronic transistor, (ii) thermal logic gates, and, as well, (iii) a thermal memory. The physical concept of these salient phononic building blocks is elucidated in Sec. II. The main physical feature in the functioning of such phonon devices is the occurrence of *negative differential thermal resistance* (NDTR); the latter is a direct consequence of the inherent nonlinear dynamics with its nonlinear response to an externally applied thermal bias.

In Sec. III we investigate how to put these thermal phononic concepts into action by using realistic nanoscale structures. The actual operations of such devices rest on extended molecular dynamics simulations which serve as a guide for implementing their experimental realization. The control of heat flow in the above-mentioned phononic building blocks is managed mainly by applying a *static* thermal bias. More intriguing control of transport emerges when the manipulations are made explicitly time dependent or by use of different external forces such as the application of magnetic fields. As detailed in Sec. IV such manipulation scenarios then generate new roadways toward fine-tuned control and counterintuitive response behaviors. Originally, such dynamic control was implemented for anomalous particle transport by taking the system dynamics out of equilibrium: Doing so results in intriguing phenomena such as Brownian motor (ratchetlike) transport, absolute negative mobility, and the like (Astumian and Hänggi, 2002; Hänggi, Marchesoni, and Nori, 2005; Hänggi and Marchesoni, 2009). Similar reasoning can be put to work for shuttling *heat* in appropriately designed lattice structures, as detailed in Sec. IV. In Sec. V, we summarize our main findings, discuss some additional elements for phononic concepts, and reflect on future potential and visions to advance the field of phononics from its present infancy toward a mature level.

II. PHONONICS DEVICES: THEORETICAL CONCEPTS

A. Thermal diode: Rectification of heat flow

The task of directing heat for information processing as in electronics requires a toolkit with suitable building blocks, namely, those nonlinear components that mimic the roles of diodes, transistors, and the like, known from electronic circuitry. The first challenge then is to design the blueprints for components that function for heat control analogous to the building blocks for electronics. This objective is best approached by making use of the nonlinear dynamics present in anharmonic lattice structures in combination with the implementation of a system-inherent symmetry breaking. We start with a discussion of the theoretical design for thermal diodes that rectify heat flow.

1. Two-segment thermal diode

In order to achieve thermal rectification, we exploit the nonlinear response mechanism that derives from inherent temperature-dependent power spectra. An everyday example of such a nonlinear frequency response is a playground swing when driven into its large-amplitude regime via parametric resonance. The response is optimized whenever the natural frequencies match those of the perturbations. Likewise, energy can be transported across two different segments of the spectrum when the corresponding vibrational frequency response characteristics overlap.

More precisely, whenever the power spectrum in one part of the device matches that in the neighboring part, we find that heat energy is exchanged efficiently. In the absence of such overlapping spectral properties, the exchange of energy becomes strongly diminished. In particular, the response behavior of realistic materials is typically anharmonic by nature. As a consequence, the corresponding power spectra become strongly dependent on temperature; see Appendix A.3. If an asymmetric system is composed of different parts with differing physical parameters, the resulting temperature dependences of the power spectra will differ likewise.

Based on these insights, a possible working principle of a thermal diode goes as follows: If a temperature bias makes the spectral features of different parts overlap with each other, we obtain a favorable energy exchange. In contrast, if for the opposite temperature bias the spectral properties of the different parts fail to overlap appreciably, a strong suppression of heat transfer occurs. In summary, this match or mismatch of spectral properties provides the salient mechanism for thermal rectification; see Figs. 3(b) and 3(c).

Because the power spectra of an arbitrary nonlinear material typically become temperature dependent, any asymmetric nonlinear system is expected to display an inequivalent heat transport upon reversal of the temperature bias. It is, however, not a simple task to design a device that results in physically designated and technologically feasible thermal diode properties. After investigating a series of possible setups, we designed a thermal diode model that performs efficiently over a wide range of system parameters (Li, Wang, and Casati, 2004). The blueprint of this device consists of two nonlinear segments which are weakly coupled by a linear spring with strength $k_{\rm int}$. Each segment is composed of a chain of particles in which each individual particle is coupled with its nearest neighbors by linear springs. This whole nonlinear two-segment chain is subjected to a cosinusoidal varying on-site potential; the latter is provided by the coupling to a substrate. These individual chains are therefore described by

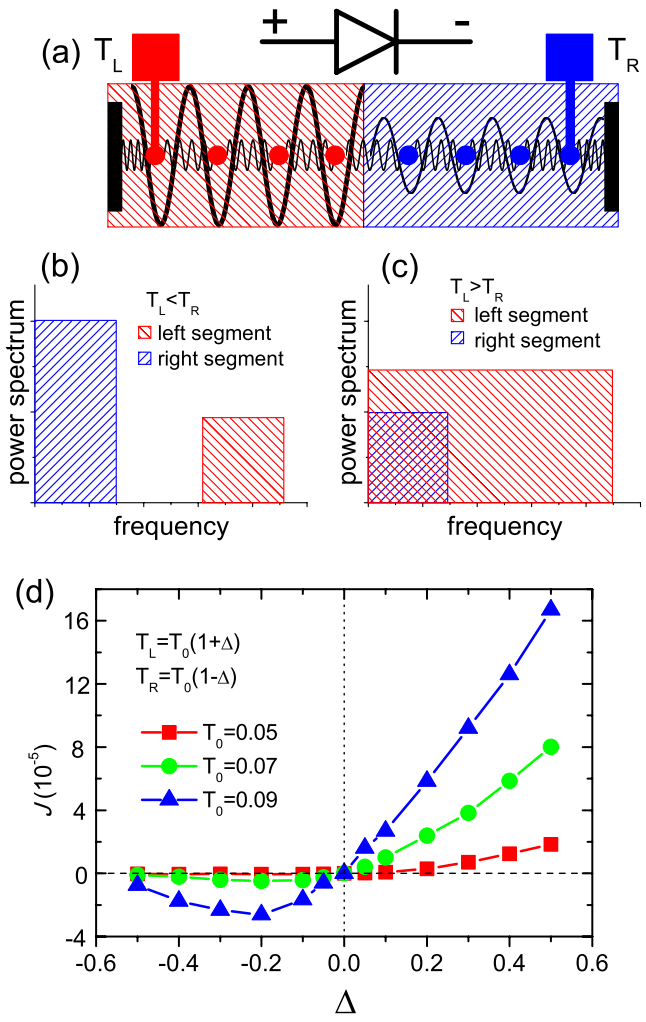

FIG. 3 (color online). Concept of a thermal diode. (a) Blueprint of an efficient two-segment thermal diode composed of two different Frenkel-Kontorova chains. The left segment consisting of a chain of particles subjected to a strong cosinusoidal varying on-site potential (illustrated by the large wavy curve) is connected to the right segment possessing a relatively weak on-site potential. (b) In the case in which the temperature T_L in the left segment is colder than the corresponding right temperature T_R, i.e., $T_L < T_R$, the power spectrum of the particle motions of the left segment is weighted at high frequencies. This occurs because of the difficulty experienced by the particles there in overcoming the large barriers of the on-site potential. In contrast, the power spectrum of the right segment is weighted at low frequencies. As a result, the overlap of the spectra is weak, implying that the heat current J becomes strongly diminished. (c) Here the situation is opposite to that in (b). With $T_L > T_R$ the particles can now move almost freely between neighboring barriers. Consequently the power spectrum extends to much lower frequencies, yielding an appreciable overlap with the right segment. This in turn causes a sizable heat current. (d) Heat current J vs the relative temperature bias Δ, as defined in the inset, for three different values of the reference temperature T_0. Adapted from Li, Wang, and Casati, 2004 and Wang and Li, 2008a.

Frenkel-Kontorova (FK) lattice dynamics; see the Appendix. The scheme of this thermal diode is depicted in Fig. 3(a).

The key feature of this FK diode setup is the chosen difference in the strengths of the corresponding on-site potentials. At low temperature, the particles are confined in the valleys of the on-site potential. Thus the power spectrum is weighted in the high-frequency regime. At high temperatures the particles assume sufficiently large kinetic energies so that thermal activation (Hänggi, Talkner, and Borkovec, 1990) across the inhibiting barriers becomes feasible. The corresponding power spectrum is then moved toward lower frequencies. By setting the strength of the on-site potential in the two segments at different levels [see Fig. 3(a)], we achieve the desired strong thermal rectification. Note that the barrier height of the on-site potential for the right segment is chosen sufficiently small so that the corresponding particles are allowed to move almost freely, both in the low- and in the high-temperature regimes. In the case that the left end is set at the low temperature, its power spectrum is weighted within the high-frequency regime. This in turn causes an appreciable mismatch with the right segment; see Fig. 3(b). In the opposite case, when the left end is set at the high temperature, its weighted power spectrum moves toward lower frequencies, thus matching well with the right segment; see Fig. 3(c).

In Fig. 3(d) the resulting stationary heat current J (see the Appendix) versus the relative temperature bias Δ is depicted for three values of the reference temperature T_0 (Li, Wang, and Casati, 2004). The relation between the dimensionless temperature and the actual physical temperature can be found in the Appendix as well. It is shown that when $\Delta > 0$ (i.e., $T_L > T_R$), the heat current gradually increases with increasing Δ, i.e., the setup behaves as a "good" thermal conductor; in contrast, when $\Delta < 0$ ($T_L < T_R$), the heat current remains small. The two-segment structure thus behaves as a "poor" thermal conductor, i.e., it mimics a thermal insulator.

For a given setup, the heat current through the system is mainly controlled by its interface coupling strength $k_{\rm int}$. Figure 4 depicts the temperature profiles for different $k_{\rm int}$ and for two oppositely chosen bias strengths. A large temperature jump occurs at the interface. The size of the jump is larger for negative bias Δ (solid symbols in Fig. 4) than for positive bias Δ. In the case with negative bias the temperature gradient inside each lattice segment almost vanishes, implying that the resulting heat current is very small. This behavior is opposite to the case with positive bias (open symbols in Fig. 4).

2. Asymmetric Kapitza resistance

The interface thermal resistance (ITR), also known as the Kapitza resistance, measures the interfacial resistance to heat flow (Pollack, 1969; Swartz and Pohl, 1989). It is defined as $R \equiv \Delta T/J$, where J is the heat flow (per area) and ΔT denotes the temperature jump between two sides of the interface. The origin of the Kapitza resistance can be traced back to the heterogeneous electronic and/or vibrational properties of the different materials making up the interface at which the energy carriers become scattered. The amount of relative transmission depends on the available energy states on each of the two sides of the interface. This phenomenon was discovered by Kapitza (1941) in experiments detecting superfluidity of He II.

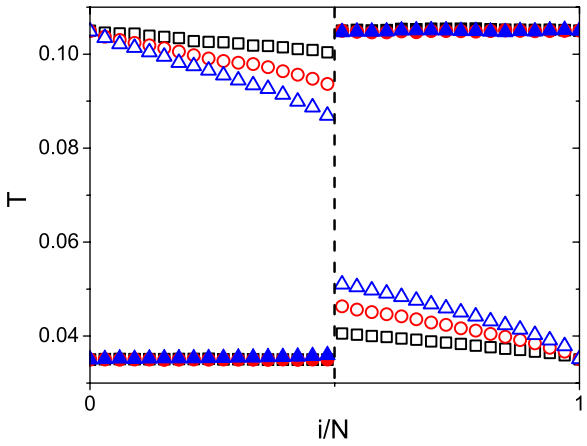

FIG. 4 (color online). Temperature profiles within a FK-FK thermal diode. The temperature profiles for various interface elastic constants $k_{\rm int} = 0.01$ (squares), 0.05 (circles), and 0.2 (triangles). $T_0 = 0.07$ and $N = 100$. The open symbols correspond to a positive temperature bias $\Delta = 0.5$, while the solid symbols correspond to a negative temperature bias $\Delta = -0.5$. The dashed line indicates the interface. The temperature jumps at the interface are due to the Kapitza resistance which is addressed in Sec. II.A.2. Adapted from Li, Wang, and Casati, 2004.

The high thermal rectification in the model setups discussed above is mainly due to this interface effect. In order to further improve the performance, Li *et al.* (2005) studied the ITR in a lattice consisting of two weakly coupled, dissimilar anharmonic segments, exemplified by a (FK) chain segment and a neighboring Fermi-Pasta-Ulam (FPU) chain segment.

Not surprisingly, the ITR in such a setup depends on the direction of the applied temperature bias. A quantity that measures the degree of overlap of the power spectra between left (L) and right (R) segments reads

$$S = \frac{\int_0^\infty P_L(\omega)P_R(\omega)d\omega}{\int_0^\infty P_L(\omega)d\omega \int_0^\infty P_R(\omega)d\omega}. \quad (1)$$

Extensive numerical simulations then reveal that $R_-/R_+ \sim (S_+/S_-)^{\delta_R}$ with $\delta_R = 1.68 \pm 0.08$, and $|J_+/J_-| \sim (S_+/S_-)^{\delta_J}$, with $\delta_J = 1.62 \pm 0.10$. The notation $+$ $(-)$ indicates the cases with a positive thermal bias $\Delta > 0$ and a negative thermal bias $\Delta < 0$, respectively. These findings thus support the strong dependence of thermal resistance on this overlap of the power spectra.

The physical mechanism of the asymmetric ITR between dissimilar anharmonic lattices can therefore be related to the match or mismatch of the corresponding power spectra. As temperature increases, the power spectrum of the FK lattice shifts downward, toward lower frequencies. In contrast, the power spectrum of the FPU segment, however, shifts upward, toward higher frequencies. Because of these opposing shifts, reversal of the thermal bias in such a FK-FPU setup can cause an even greater change in the amount of match or mismatch than in the FK-FK setup considered above. Conceptually this results in an even stronger thermal rectification.

B. Negative differential thermal resistance: The thermal transistor

The design and the experimental realization of the thermal diode present a striking first step toward the goal of using phononics. The next challenge to be overcome is a design for a thermal transistor, which allows for an *a priori* control of heat flow similar to the familiar control of charge flow in a field-effect transistor. Similar to its electronic counterpart, a thermal transistor consists of three terminals: the drain (D), the source (S), and the gate (G). When a constant temperature bias is applied between the drain and the source, the thermal current flowing between the source and the drain can be fine-tuned by the temperature that is applied to the gate. Most importantly, because the transistor is able to amplify a signal, the changes in the heat current through the gate can induce an even larger current change from the drain to the source.

Toward the eventual realization of such a thermal transistor device we consider the concept depicted in Fig. 5(a). It uses a one-dimensional anharmonic lattice structure where the temperatures at its ends are fixed at T_D and T_S ($T_D > T_S$), respectively. An additional, third heat bath at temperature T_O controls the temperature at node O, so as to control the two heat currents J_D and $J_S = J_D + J_O$. Next we define the current amplification factor α. This quantity describes the amplification ability of the thermal transistor as the change of the heat current J_D (or J_S, respectively), divided by the change in gate current J_O, which acts as the control signal. This amplification quantity explicitly reads

$$\alpha = |\partial J_D/\partial J_O|. \tag{2}$$

Equation (2) can be recast in terms of the differential thermal resistance of the segment S, i.e.,

$$r_S \equiv (\partial J_S/\partial T_O)^{-1}_{T_S=\text{const}}, \tag{3}$$

and that of the neighboring segment D, i.e.,

$$r_D \equiv -(\partial J_D/\partial T_O)^{-1}_{T_D=\text{const}}, \tag{4}$$

to yield

$$\alpha = |r_S/(r_S + r_D)|. \tag{5}$$

It can readily be deduced that if r_S and r_D are both positive then α is less than unity. Consequently, such a thermal transistor cannot work.

For a transistor to work it is thus necessary that the current amplification factor obeys $\alpha > 1$. This implies a NDTR; i.e., it requires a transport regime wherein the heat current *decreases* with *increasing* thermal bias. Such behavior occurs with the thermal diode characteristics depicted in Fig. 3(d); note the behavior for the case with solid triangles with Δ in the range of $[-0.5, -0.2]$. It should be pointed out that such a (NDTR) behavior is in no conflict with any physical laws.[1]

While negative differential electric resistance has long been realized and extensively studied (Esaki, 1958), the concept of NDTR was proposed only more recently (Li, Wang, and Casati, 2004; 2006). With temperature T_O increasing, the match between sensitively temperature-dependent power spectra of the two segments becomes increasingly better, which not only offsets the effect of a decreasing thermal bias ($T_D - T_O$) but even induces an increasing heat current. This behavior is illustrated in Fig. 5(b).

A system displaying NDTR constitutes the main ingredient for operation of a thermal transistor. The scheme of a thermal transistor is shown in Fig. 6(a). In order to make this setup physically more realistic, a third segment (G) is connected to the node O. This is done because in an actual device it is difficult to directly control the temperature of node O, which is located inside the device. Using different sets of parameters, this thermal transistor can work either as a thermal switch [see Fig. 6(b)], or as a thermal modulator [see Fig. 6(c)].

The key prerequisite for a thermal transistor, i.e., the NDTR phenomenon, has been investigated in various other systems recently, e.g., for high-dimensional lattice models (Lo, Wang, and Li, 2008). A gas-liquid transition was also utilized in the design of a thermal transistor (Komatsu and Ito, 2011). The condition for the existence of a NDTR regime is more stringent than that of obtaining merely thermal rectification.

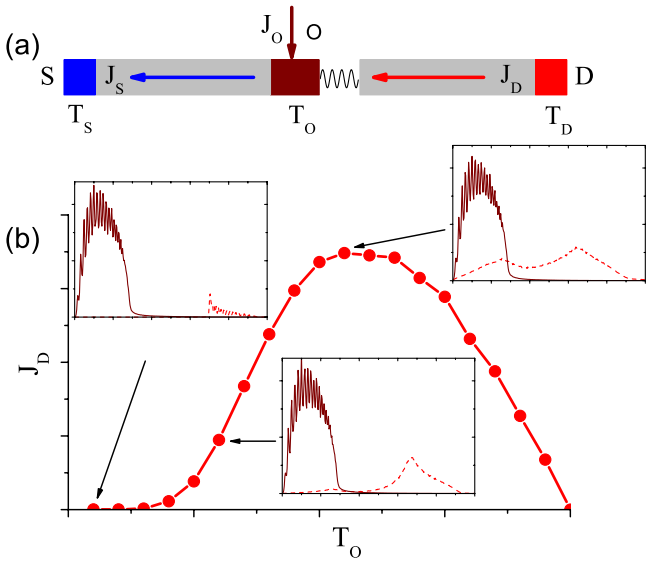

FIG. 5 (color online). Concept of a thermal transistor. (a) A one-dimensional lattice is coupled at its two ends to heat baths at temperatures T_D and T_S with $T_D > T_S$. A third heat bath with temperature $T_S < T_O < T_D$ can be used to control the temperature at the node O, so as to control the heat currents J_D and J_S. (b) In an extended regime, as the temperature T_O increases, the thermal bias ($T_D - T_O$) at the interface decreases while the power spectrum in the left segment of the control node increasingly matches with the power spectrum of the neighboring segment that is connected to the drain D. This behavior is depicted in the insets where the corresponding power spectra of the left-side and right-side interface particles are depicted for three representative values of T_O, as shown by the three arrows. The resulting drain current J_D increases with increasing overlap until it reaches a maximum and starts to decrease again.

[1]Note that this NDTR should not be confused with absolute negative thermal resistance around an equilibrium working point at thermal bias $\Delta = 0$. The latter implies that heat flows from cold to hot which violates the principle of Le Chatelier-Brown (Callen, 1960), i.e., no *opposite* response to a small external perturbation around a thermal equilibrium is possible. Such an anomalous response behavior is, however, feasible when the system is taken (at a zero bias) into a stationary nonequilibrium state (Hänggi and Marchesoni, 2009).

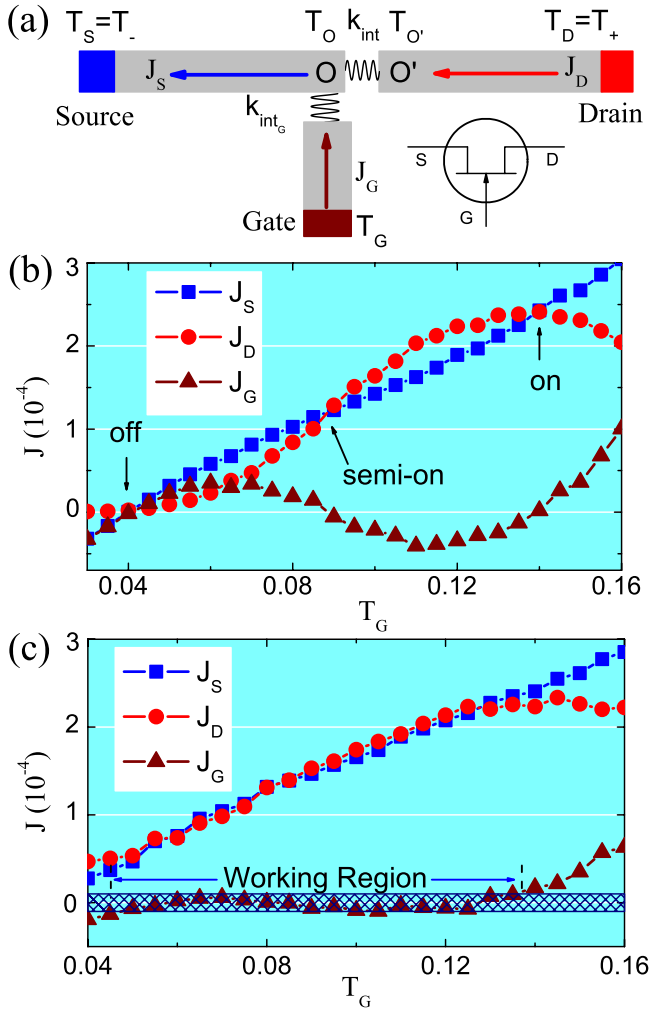

FIG. 6 (color online). Thermal transistor. (a) Sketch of a thermal transistor device. Just as in the case of an electronic transistor, it consists of two segments (the source and the drain) and, as well, a third segment (the gate) where the control signal is injected. The temperatures T_D and T_S are fixed at high, T_+, and low, T_-, values. Negative differential thermal resistance (NDTR) occurs at the interface between O and O'. This then makes it possible that, over a wide regime of parameters, when the gate temperature T_G rises, not only J_S but also J_D may increase. Use of different system parameters then allows different functions, this being either a thermal switch (b) or a thermal modulator (c). (b) Function of a thermal switch: At three working points where $T_G = 0.04$, 0.09, and 0.14, the heat current J_D equals J_S, so that $J_G = J_S - J_D$ vanishes identically. These three working points correspond to (stable) "off," (unstable) "semi-on," and (stable) "on" states, at which J_D differs substantially. We can switch, i.e., forbid or allow heat flowing by setting T_G at these different values. (c) Function of a thermal modulator. Over a wide temperature interval of gate temperature T_G, depicted via the hatched working region, the heat current J_G remains very small, i.e., it remains inside the hatched regime, while the two heat currents J_S and J_D can be continuously controlled from low to high values. Adapted from Li, Wang, and Casati, 2006.

The crossover from existence to nonexistence of NDTR was investigated for a set of different lattice structures, by both analytical and numerical means (He, Buyukdagli, and Hu, 2009; Shao *et al.*, 2009). Because the NDTR in these lattice models is basically derived from an interface effect, it is plausible that, with a too large interface coupling strength $k_{\rm int}$ or a too long lattice length, it is rather the thermal resistance of the involved segments than the interface resistance that rules the NDTR. As a consequence, the NDTR effect typically becomes considerably suppressed. We therefore expect that NDTR can experimentally be realized with nanoscale materials, for example, using nanotubes, nanowires, etc.; see Chang *et al.* (2006, 2007, 2008). This issue is addressed in greater detail in Sec. III.

C. Thermal logic gates

The phenomenon of NDTR not only provides the function for thermal switching and thermal modulation, but also is the essential input in devising thermal logic gates. Setups for all major thermal logic gates able to perform logic operations have been put forward recently (Wang and Li, 2007).

In digital electric circuits, two Boolean states 1 and 0 are encoded by two different values of voltage, while in a digital thermal circuit these Boolean states can be defined by two different values of temperature $T_{\rm on}$ and $T_{\rm off}$. In the following we discuss how to realize such individual logic gates.

The most fundamental logic gate is a signal repeater which "digitizes" the input. That is, when the input temperature is lower (higher) than a critical value T_c, with $T_{\rm off} < T_c < T_{\rm on}$, the output is set at $T_{\rm off}$ ($T_{\rm on}$). This is not a simple task; it must take into account that small errors may accumulate, thus leading eventually to incorrect outputs.

The thermal repeater can be obtained by use of thermal switches. We inspect again the thermal switch shown in Fig. 6(a), in which the T_G dependence of the heat currents J_D, J_S, and J_G is illustrated in Fig. 6(b). When the gate temperature T_G is set very close to but not precisely at $T_{\rm off}$ or $T_{\rm on}$, the heat current in the gate segment makes the temperature in the junction node O approach $T_{\rm off}$ or $T_{\rm on}$ more closely. Therefore, when such switches are connected in series, which involves plugging the output (from node O) of one switch into the gate of the next one, the final output will asymptotically approach that of an ideal repeater, i.e. $T_{\rm on}$ or $T_{\rm off}$, whichever is closer to the input temperature T_G.

A NOT gate reverses the input; it yields the response 1 whenever it receives 0, and vice versa. This requires that the output temperature falls when the input temperature rises, and vice versa. This feature can be realized by injecting the signal from the node G and collecting the output from the node O'; cf. Fig. 6(a). The NDTR between the nodes O and O' again plays the key role. A higher temperature T_G induces a larger thermal current J_D and therefore increases the temperature bias in segment D. $T_{O'}$ thus decreases (note that T_D is fixed) and a negative response is thus realized; cf. Fig. 7(a). Suppose $T_{O'}$ equals $T_{O'}^{\rm off}$ and $T_{O'}^{\rm on}$, with $T_{O'}^{\rm off} > T_{O'}^{\rm on}$, when T_G equals $T_{\rm off}$ and $T_{\rm on}$, respectively. A remaining problem is that both $T_{O'}^{\rm off}$ and $T_{O'}^{\rm on}$ are higher than T_c (in fact even higher than $T_{\rm on}$). This in turn will always be treated as a logical 1 by the following device. This problem can be solved if we apply a "temperature divider," the counterpart of a voltage divider, which is depicted in the inset of Fig. 7(b). Its output is a fraction of its input. By adjusting this fraction, we can make the output of the temperature divider higher or lower than T_c when its input equals $T_{O'}^{\rm off}$ or $T_{O'}^{\rm on}$. We then employ a thermal repeater to digitize the output

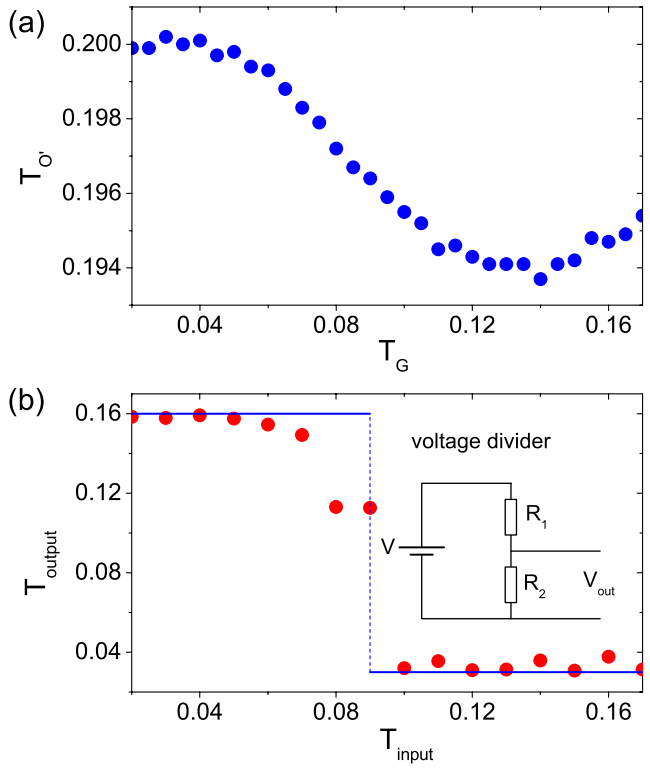

FIG. 7 (color online). Negative response and thermal NOT gate. (a) Temperature of the node O' as a function of T_G for the setup shown in Fig. 6(a). In a wide range of T_G, $T_{O'}$ decreases as T_G increases. (b) Function of the thermal NOT gate. The thin line indicates the function of an ideal NOT gate. Inset: Structure of a two-resistor voltage divider, the counterpart of a temperature divider, which supplies a voltage lower than that of the battery. The output of the voltage divider is $V_{\text{out}} = VR_2/(R_1 + R_2)$. Adapted from Wang and Li, 2007.

from the temperature divider. In doing this the function of a NOT gate is therefore realized, as depicted in Fig. 7(b).

Similarly, an AND gate is a three-terminal (two inputs and one output) device. The output is 0 if either of the inputs is 0. Because we now have the thermal signal repeater at our disposal, an AND gate is readily realized by plugging two inputs into the same repeater. It is clear that when both inputs are 1, then the output is also 1; and when both inputs are 0, then the output is also 0. By adjusting some parameters of the repeater, we are able to make the final output 0 when the two inputs are opposite, therefore realizing a thermal AND gate. An OR gate, which exports 1 whenever the two inputs are opposite, can also be realized in a similar way.

D. Thermal memory

Toward the goal of an all-phononic computing, other indispensable elements, besides thermal logic gates, are thermal memory elements that enable the storage of information via its encoding by heat or temperature. One possible setup acting as a thermal memory was proposed by Wang and Li (2008b). Its blueprint has much in common with the working scheme for the thermal transistor of Fig. 6(a). By appropriate adjustment of parameters, negative differential thermal resistance can be induced between the chain segments connecting to node O and node O', respectively. With fixed T_S and T_D, obeying $T_S < T_D$, and a heat bath at temperature T_G that is coupled to the node G, three possible working points for T_G, i.e., T_{off}, $T_{\text{semi-on}}$, and T_{on}, can be realized. At these three working points the gate current vanishes, $J_G = 0$, thus perfectly balancing J_S and J_D. Analysis of the slope of J_G at these points shows that two of these, i.e., (T_{off}, T_{on}), denote stable working points and the intermediate one $T_{\text{semi-on}}$ is unstable. Notably, these working states remain stationary when the heat bath that is coupled to terminal G is removed. Now, however, the corresponding temperatures at these working points exhibit fluctuations. As well known from stochastic bistability (Hänggi, Talkner, and Borkovec, 1990), small fluctuations around these working points drive the system consistently back to the stable working points and away from the unstable working point. Accordingly, the system possesses two long-lived metastable states, $T_O = T_{\text{on}}$ and $T_O = T_{\text{off}}$, while $T_O = T_{\text{semi-on}}$ is unstable.

The stability of these thermal states at T_{on} and T_{off}, adjusted in this way, implies that these states remain basically unchanged over an extended time span in spite of thermal fluctuations. This holds true even if a small external perturbation, as, for example, imposed by a small thermometer reading the temperature at the node O, is applied.

The working principle of a write-and-read cycle of such a thermal memory is depicted in Fig. 8: Starting out at time $t = 0$ from a random initial preparation of all particles making up the memory device, the local temperature at site O relaxes to its stationary value $T_O \sim 0.18$ (initializing stage). For the case in Fig. 8(b) the writer, prepared at its Boolean temperature value T_{off}, is next connected to site O (writing stage). As can be deduced from Fig. 8(b), the temperature T_O quickly relaxes during this writing cycle to this Boolean value and maintains this value over an extended time span, even after the writer is removed (maintaining stage). More importantly, T_O self-recovers to this setting temperature T_{off} after being exposed to the small perturbation induced by the reader (a small thermometer) during the subsequent data-reading stage. The data stored in the thermal memory are therefore precisely read out without destroying the memory state.

In Fig. 8(c), the write-and-read process corresponding to the opposite Boolean writing temperature value, i.e., $T_O = T_{\text{on}}$, is depicted. Accordingly, this engineered write-and-read cycle with its two possible writing temperatures T_{off} and T_{on} accomplishes the task of a thermal memory device.

III. PUTTING PHONONS TO WORK

In Sec. II, we investigated various setups involving stylized nonlinear lattice structures in order to manipulate heat flow. We next discuss how to put these concepts into practical use with physically realistic systems. In doing so we consider numerical studies of suitably designed nanostructures which exhibit the designated thermal rectification properties. This discussion is then followed by the first experimental realizations of a thermal diode and thermal memory.

Among the many physical materials that come to mind, low-dimensional nanostructures such as nanotubes, nanowires, and graphene likely offer optimal choices to realize the desired thermal rectification features obtained in nonlinear lattice

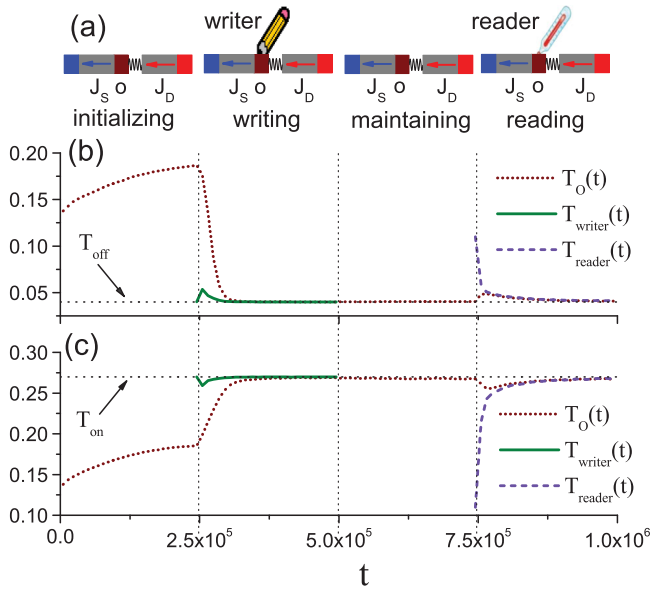

FIG. 8 (color). Write-and-read cycle in a thermal memory. (a) Illustration of the four stages of a complete writing-reading process. The left and right ends of this thermal memory are coupled to heat baths at fixed temperatures $T = 0.03$ and 0.3, respectively. During the initializing stage the system relaxes toward its stationary state with the temperature at site O being $T_O = 0.18$. The different stages during this cycle are indicated by dashed vertical lines in (b) and (c). (b) Time evolution of the local temperature $T_O(t)$ (dotted wine color) of the central particle at site O, the temperature of the writer $T_{\text{writer}}(t)$ (solid), and the temperature of the reader $T_{\text{reader}}(t)$ (dashed) during a complete write-and-read process. The time-dependent local temperature of the particle (with unit mass) at site O is obtained by integrating and averaging the squared velocity $v_O^2(t)$ over a short time span (10^4 time units), centered at time instant t. The writer and reader are realized with short lattice segments, while T_{writer} and T_{reader} are the averaged temperatures of all particles within the writer and reader, respectively. During the writing stage the node O is coupled to one end of the writer, whose opposite end is coupled to a heat bath set at the off value $T_{\text{off}} = 0.04$. During the reading stage, the reader set at initial temperature 0.11 is attached to the node O. (c) The opposite write-and-read cycle with the writer set at the on value with $T_{\text{on}} = 0.27$. Adapted from Wang and Li, 2008b.

studies. It is known from theoretical studies (Lepri, Livi, and Politi, 2003; Dhar, 2008; Saito and Dhar, 2010) and experimental validation (Chang *et al.*, 2008; Ghosh *et al.*, 2010) that the characteristics of heat flow [such as the validity of the Fourier law (Lepri, Livi, and Politi, 2003; Dhar, 2008; Saito and Dhar, 2010)] sensitively depend on spatial dimensionality and the absence or presence of (momentum) conservation laws.

This is even more strongly the case for nanomaterials, where due to the limited size, the discrete phonon spectrum (Yang, Zhang, and Li, 2010) results in a distinct dependence of the thermal quantities on the specific geometrical configuration, mass distribution, and ambient temperature. Overall, this makes nanosized materials promising candidates for phononics. Because the experimental determination of thermal transport properties is not straightforward, the combined use of theory and numerical simulation is indispensable in devising phononics devices. Moreover, novel atomistic computational algorithms have been developed which facilitate the study of experimentally relevant system sizes (Li *et al.*, 2010).

A. Thermal diodes from asymmetric nanostructures

Carbon nanotubes (CNTs) recently attracted attention for applications in nanoscale electronic, mechanical, and thermal devices. CNTs possess a high thermal conductivity at room temperature (Kim *et al.*, 2001) and phonon mean free paths that extend over the length scale of structural ripples, thus providing ideal phonon waveguide properties (Chang *et al.*, 2007).

Consider thermal rectification in junctions based on single-walled carbon nanotubes (SWCNTs) junctions (Wu and Li, 2007). A typical $(n, 0)/(2n, 0)$ intramolecular junction structure is shown in Fig. 9(a) in which the structure contains two parts, namely, a segment with an $(n, 0)$ SWCNT and a segment made of a $(2n, 0)$ SWCNT. These two segments are connected by m pairs of pentagon-heptagon defects. By use of nonequilibrium molecular dynamics (NEMD) simulations, one finds that the heat flux from the $(2n, 0)$ to the $(n, 0)$ tube exceeds that from the $(n, 0)$ tube to the $(2n, 0)$ segment. The corresponding thermal rectification increases upon raising the temperature bias.

Another beneficial feature is that the rectification is only weakly dependent on the detailed structure of the interface, assuming that the connecting region is sufficiently short. This occurs because heat is predominantly carried by long-wavelength phonons, which are scattered mainly by large defects. Just as with nonlinear lattice models, the match or mismatch of the energy spectra around the interface is the underlying mechanism for rectification. Furthermore, in the elongated structure (Wu and Li, 2008) the heat flux becomes smaller than that of the nondeformed structure; its temperature dependence, however, becomes more pronounced, due to the intrinsic tensile stress.

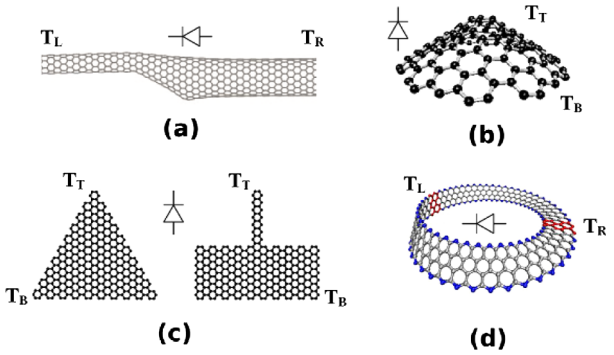

FIG. 9 (color online). Schematic system setups for thermal diodes devised from asymmetric nanostructures: (a) a typical $(n, 0)/(2n, 0)$ carbon nanotube junction; (b) a carbon-nanocone-based thermal rectifier; (c) two asymmetric graphene nanoribbons (GNRs), a trapezium-shaped GNR, and, as well, a structure made of two rectangular GNRs of different widths; (d) a topological configuration based on a Möbius graphene stripe. The parts (T_L and T_R) denote the corresponding heat bath regions. The bath temperatures of the two ends are denoted as T_T (top) and T_B (bottom) in (b) and (c), and as T_L (left) and T_R (right) in (a) and (d), respectively. Adapted from Wu and Li, 2007, Yang, Zhang, and Li, 2008, 2009, and Jiang, Wang, and Li, 2010.

The carbon nanocone depicted in Fig. 9(b) is yet another carbon-based material exhibiting a high asymmetric geometry. Its thermal properties were investigated by Yang, Zhang, and Li (2008). A temperature difference Δ between the two ends of the nanocone is introduced; it is positive when the bottom of nanocone is at a higher temperature and negative in the opposite case. It was found that the nanocone behaves as a good thermal conductor under positive thermal bias and as a poor thermal conductor when exposed to a negative thermal bias. This suggests that the heat flux runs preferentially along the direction of decreasing diameter.

In order to compare the impact of mass asymmetry versus geometry asymmetry for thermal rectification, a nanocone structure with a graded mass distribution was discussed (Yang, Zhang, and Li, 2008). The mass of the atoms of the nanocone was devised to change linearly; that is, the top atoms possess a minimum mass $M_{^{12}\mathrm{C}}$ and the bottom atoms have the maximum mass of $4M_{^{12}\mathrm{C}}$, with $M_{^{12}\mathrm{C}}$ being the mass of the ^{12}C atom. NEMD results then yield a rectification ratio $|J_+ - J_-|/|J_-|$ that is 10% for a nanocone with uniform masses and 12% for the mass-graded nanocone (at identical thermal bias Δ). This 2% increase for the mass-graded distribution evidences that the role of geometric asymmetry is more effective in boosting thermal rectification.

These geometric asymmetric SWCNT junctions all exhibit thermal rectification. Compared to the SWCNT setup, it is easier, however, to control the shape of graphene by nanocutting technology such as a helium ion microscope. Graphene nanoribbons (GNRs) [see Fig. 9(c)] present promising elements for nanoelectronics and nanophononics. For instance, Yang, Zhang, and Li (2009) demonstrated tunable thermal conduction in GNRs. They studied the direction-dependent heat flux in asymmetric structural GNRs and explored the impacts of both, GNR shape and size on the rectification ratio. Two types of GNR were considered: trapezium-shaped GNRs and GNRs composed of two rectangles of different widths; see Fig. 9(c).

These two types of GNR behave as good thermal conductors under positive thermal bias (i.e., bottom end at higher temperature) and as poor thermal conductors under negative thermal bias (i.e., top end at higher temperature). This finding is similar to the rectification phenomenon observed in carbon-nanocone structures (Yang, Zhang, and Li, 2008), which again results from the amount of match or mismatch between the respective phonon spectra.

It is interesting to note that the rectification ratios of GNRs are substantially larger than those in nanocone and SWCNT junctions. With $\Delta = 0.5$, the rectification ratio of the nanocone is 96% (Yang, Zhang, and Li, 2008) and that of the SWCNT intramolecular junction is only around 15% (Wu and Li, 2007), while the rectification ratio in GNRs is about 270% and 350% for two-rectangle GNRs and trapezium-shaped GNRs, respectively. The rectification ratio of the trapezium-shaped GNR is thus larger than that of the two-rectangle GNR under the same thermal bias difference. This feature is consistent with the phenomenon that the carbon nanocone (i.e., the geometric graded structure) possesses a larger rectification ratio than the two-segment carbon nanotube $(n, 0)/(2n, 0)$ intramolecular junction. The phonon spectra change continuously in the graded structures, which implies a more efficient control of heat flux. Similar rectification features were observed in graphene nanoribbons by Hu, Ruan, and Chen (2009).

Yet another advantage of a GNR-based thermal rectifier is its weak dependence on length. Because energy is transported ballistically in graphene, the heat flux is essentially independent of size. Both J_+ and J_- are saturated when the GNR length is greater than $\sim$5.1 nm, so that the rectification ratio remains constant around 92%. Moreover, compared to a setup composed of a single-layer graphene, an even larger rectification ratio can be achieved in few-layer asymmetric structures, this being a consequence of layer-layer interactions (Zhang and Zhang, 2011).

Thermal rectification can also be realized with a topological graphene setup such as the Möbius graphene strip (Jiang, Wang, and Li, 2010); see Fig. 9(d). The advantage of this topology-induced thermal rectification is that it is practically insensitive to the temperature and size of the system. In this structure, the asymmetry originates from the intrinsic topological configuration.

Because phonons are strongly scattered due to the mismatch in vibrational properties of the materials forming the interface, which in addition depends on the sign of the applied thermal bias, this produces an asymmetric Kapitza contact resistance. Capitalizing on this idea, an amorphous-silicon–polyethylene thermal rectifier was designed (Hu, Keblinski, and Li, 2008), in which the heat current from the polymer to the silicon is larger than vice versa. To examine the origin of the thermal rectification, the density of states of phonons on each side of the interface was investigated. The phonon density of states significantly softens in the polymer as it becomes warmer. This increases the density of states in the polymer at low frequencies. Thus the transmission probability of those low-frequency acoustic modes in silicon increases, yielding an enhanced thermal transport.

The setups discussed thus far are all operating in steady state. A transient thermal transport exhibiting a time-dependent thermal rectification was investigated for a Y-SWCNT junction by Gonzalez Noya, Srivastava, and Menon (2009). From their molecular dynamics simulation it is reported that a heat pulse propagates unimpeded from the stem to the branches, undergoing little reflection. For the reverse temperature bias, however, there is a substantial reflection back into the branches. The transmission coefficient from the stem to the branches is more than 4 times that of the reverse direction.

We reflect again on the choice of materials suitable for obtaining those theoretically predicted thermal rectification features. A thermal rectifier constitutes a two-terminal thermal device whose working principle rests upon the different overlap of the temperature-dependent phonon spectra. For this to occur strong anharmonicity is an important factor. Given the above discussion of geometric asymmetric structures, a strong intrinsic anharmonicity corresponds to diffusive phonon transport. However, diffusive phonon transport is not a necessary condition for thermal rectification. In asymmetric GNRs, phonon transport is almost ballistic. The conclusion is that thermal rectification exists for both ballistic and diffusive phonon transport, assuming that a mismatch of the phonon spectrum of the two ends is present. This difference in phonon spectra can originate from different sources, such as, for example, from an

asymmetric mass distribution, different geometry, size, or spatial dimension.

Despite an abundance of parameter-dependent rectification studies (Hu *et al.*, 2006; Yang *et al.*, 2007; Wu and Segal, 2009; Wu, Yu, and Segal, 2009), these have rarely been tested against experiments. All these NEMD studies rely on mathematically idealized material Hamiltonians, which in practice may still be far from physical reality. Only *in situ* experiments thus present the ultimate test bed for a validation of the wealth of available theoretical results and, even more importantly, dictate the necessary next steps toward an implementation of phononics.

B. *In situ* thermal diodes from mass-graded nanotubes: Experiment

On the experimental side, a pioneering work on thermal diodes was performed by Chang *et al.* (2006). In their experiment (cf. Fig. 10), CNTs and boron nitride nanotubes (BNNTs) were gradually deposited on a surface with the heavy molecules located along the length of the nanotube in order to establish an asymmetric mass distribution. As an important test, it was experimentally checked that in unmodified NTs with uniform mass distribution the thermal conductance is indeed *independent* of the direction of the applied thermal bias. In clear contrast, however, the inhomogeneous NT system in fact does exhibit asymmetric axial thermal conductance, with greater heat flow in the direction of decreasing mass density. The thermal rectification ratios, i.e., $|J_+ - J_-|/|J_-|$, were measured as 2% and 7% for CNTs and BNNTs, respectively. The higher thermal rectification found in BNNTs might originate from stronger nonlinearity, as induced by the ionic nature of the B-N bonds, which in turn favors thermal rectification.

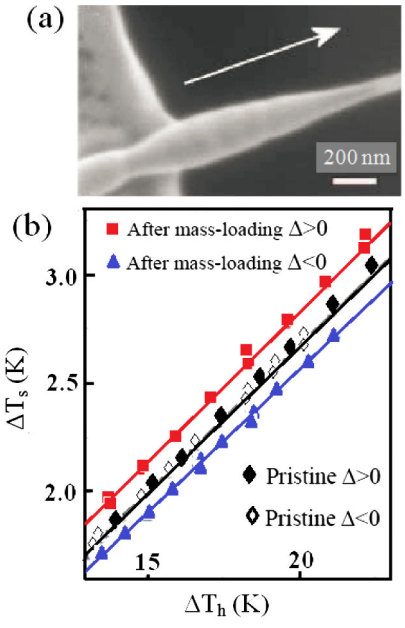

FIG. 10 (color online). Experimental realization of thermal rectification in nanotube junctions. (a) Scanning-electron-microscope images of boron nitride nanotubes (BNNTs) after deposition of $C_9H_{16}Pt$. (b) Graphical representation of the temperature changes of the heater (ΔT_h) and sensor (ΔT_s) for the nanotubes before and after deposition of $C_9H_{16}Pt$. Adapted from Chang *et al.*, 2006.

In order to understand the mechanism of rectification in the experiment of Chang *et al.*, subsequent work (Yang *et al.*, 2007) studied the thermal properties in a one-dimensional anharmonic lattice with a mass gradient. Yang *et al.* (2007) found that in the 1D mass-graded chain, when the heavy-mass end is set at high temperature, the heat flux is larger than that under the reverse temperature bias. This is consistent with the experimental results of Chang *et al.* (2006). Also, the larger is the mass gradient, the larger is the thermal rectification. As mentioned, this can be explained by differences in overlap of the respective phonon power spectra.

C. Solid-state-based thermal memory: Experiment

Apart from the experimental demonstration of a nanoscale thermal rectifier, a thermal memory device was recently also brought into operation experimentally by Xie *et al.* (2011). In their work [see Fig. 11(a)], a single-crystalline VO_2 nanobeam is used to store and retain thermal information with two temperature states as input T_{in} and output T_{out}, which serve as the logical Boolean units 1 (= high) and 0 (= low), for writing and reading. This has been achieved by exploiting a metal-insulator transition. A nonlinear hysteretic response in temperature was obtained in this way. A voltage bias across the nanobeam was applied to tune the characteristics of the thermal memory. One finds that the hysteresis loop becomes substantially enlarged [see Fig. 11(b)] and is shifted toward lower temperatures with increasing voltage bias. Moreover, the difference in the output temperature T_{out} between its high- and low-temperature states increases substantially with increasing voltage bias. To demonstrate the repeatability of the thermal memory, they performed repeated write(high)-read-write(low)-read cycles using heating and cooling pulses to the input terminal [see Fig. 11(c) for more details]. Repeated cycling over 150 times proves the reliable and repeatable performance of this thermal memory.

IV. SHUTTLING HEAT AND BEYOND

The function of the various thermal electronic analog devices discussed in Sec. II used a heat control mechanism which is based on a static thermal bias. In order to obtain an even more flexible control of heat energy, comparable with the richness available for electronics, one may design intriguing phononic devices which utilize temporal, ac gating modulations as well. Such forcing makes possible the realization of a plenitude of novel phenomena such as the heat ratchet effect, absolute negative heat conductance, or the realization of Brownian (heat) motors, to name but a few (Astumian and Hänggi, 2002; Hänggi, Marchesoni, and Nori, 2005; Hänggi and Marchesoni, 2009). Among the necessary prerequisites to run such heat machinery are thermal noise, nonlinearity, unbiased nonequilibrium driving of deterministic or stochastic nature, and a symmetry-breaking mechanism. This then carries the setup away from thermal equilibrium, thereby circumventing the second law of thermodynamics, which otherwise imposes a vanishing directed transport (Hänggi and Marchesoni, 2009).

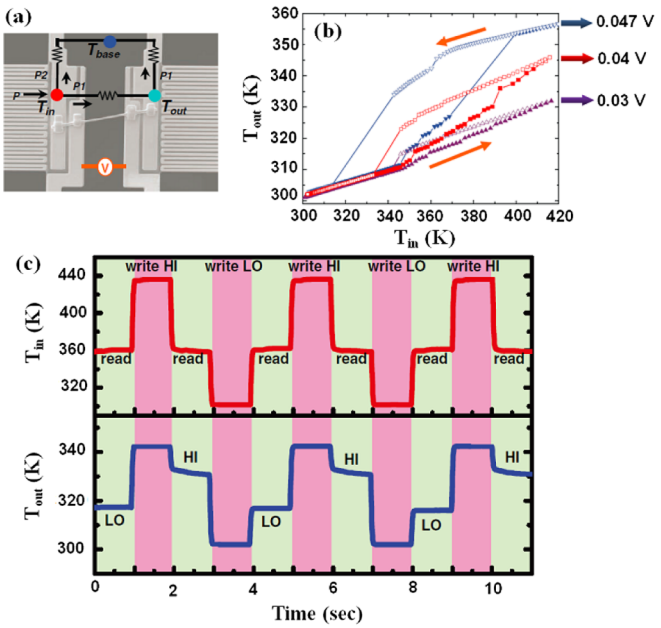

FIG. 11 (color online). Experimental realization of the thermal memory. (a) Scanning-electron-microscope image of the memory device, consisting of a VO_2 nanobeam connecting the input terminal (left side) and output terminal (right side). An equivalent thermal circuit is also depicted in the image. (b) Output temperature T_{out} as a function of input temperature T_{in}, upon heating (solid symbols) and cooling (open symbols). The characteristics of the thermal memory are tuned under three different voltage biases, as indicated. (c) Write-and-readout process of logical 1 (= high-temperature state) and 0 (= low-temperature state). Upper part, $T_{in}(t)$ for writing: To write a high- (= 1) temperature state to the output terminal, a heating pulse generated by increasing the heating current was applied to the input terminal to set T_{in} to 435 K. To switch the output terminal to a low-temperature state, a cooling pulse was applied to the input terminal to set T_{in} to 300 K by natural cooling of T_{in} to the substrate temperature T_{base}. Lower part, $T_{out}(t)$ for reading: When T_{in} was returned to 360 K for reading, the high- (low-) temperature of $\sim 332.1 \pm 0.1$ K ($\sim 317 \pm 0.8$ K) was retained and could be read out at the output terminal T_{out}. Here the voltage bias is 0.04 V. Adapted from Xie *et al.*, 2011.

Dwelling on similar ideas used in Brownian motors for directing particle flow, an efficient pumping or shuttling of energy across spatially extended nanostructures can be realized by modulating either one or more thermal bath temperatures, or by applying external time-dependent fields, such as mechanical, electric, or magnetic forces. This gives rise to intriguing phononic phenomena such as *a priori* directed shuttling of heat *against* an external thermal bias or the pumping of heat that is assisted by a geometrical-topological component.

A. Classical heat shuttling

In the following we elucidate the objective for shuttling heat against an externally applied thermal bias. A salient requirement for the *modus operandi* of heat motors is the presence of a spatial or dynamic symmetry breaking.

A possible scenario consists of coupling an asymmetric nonlinear structure to two baths; i.e., a left (L) and right (R) heat bath which can be modeled by classical Langevin dynamics. Application of a periodically time-varying temperature in one or both heat baths, $T_{L(R)}(t) = T_{L(R)}(t + 2\pi/\omega)$, possessing the same average temperature $\overline{T_{L(R)}(t)} = T_0$, then brings the system out of equilibrium. It is noteworthy that this driven system is unbiased; i.e., it exhibits a vanishing average thermal bias $\overline{\Delta T(t)} = \overline{T_L(t) - T_R(t)} = 0$. The asymptotic heat flux $J(t)$ assumes the periodicity of the external driving period $2\pi/\omega$ and the time-averaged heat flux J follows as the cycle average over a full temporal period $J = (\omega/2\pi)\int_0^{2\pi/\omega} J(t)dt$. Consequently, a nonzero average heat flux $J \neq 0$ emerges which then provides the seed to shuttle heat against a net thermal bias $\overline{\Delta T(t)} \neq 0$.

A first possibility to introduce the necessary symmetry breaking is to use an asymmetric material such as two coupled FK-FK lattices where the two segments possess different thermal properties (Li, Hänggi, and Li, 2008; Ren and Li, 2010); see Fig. 12. The directed heat transport can be extracted from unbiased temperature fluctuations by harvesting the static thermal rectification effect (Li, Wang, and Casati, 2004).

Yet another possibility is to break the symmetry dynamically by exploiting the nonlinear response induced by the harmonic mixing mechanism, stemming from a time-varying two-mode modulation of the bath temperature(s), i.e., $T_{L(R)}(t) = T_0[1 \pm A_1\cos(\omega t) \pm A_2\cos(2\omega t + \varphi)]$. The second harmonic driving term $A_2\cos(2\omega t + \varphi)$ causes the intended nonlinear frequency mixing (Li *et al.*, 2009).

In the adiabatic limit, i.e., if $\omega \to 0$, a nonzero heat flux $J \neq 0$ can be obtained due to the nonlinearity of the heat conductance response. The preferred direction of such heat flow is determined by the intrinsic thermal diode properties. In contrast, in the fast-driving limit $\omega \to \infty$, the left and right ends of the system will essentially experience a time-averaged constant temperature. This then mimics thermal equilibrium, yielding $J \to 0$. Remarkably, by modulating the driving frequency ω through the characteristic thermal

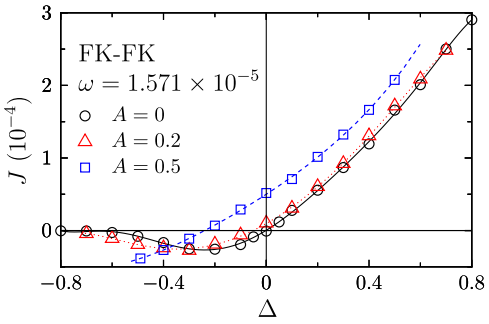

FIG. 12 (color online). Action of a heat Brownian motor in two coupled asymmetric FK-FK lattices. The heat baths are subjected to periodic modulations in the forms $T_L(t) = T_0[1 + \Delta + A\,\mathrm{sgn}(\sin\omega t)]$ and $T_R(t) = T_0(1 - \Delta)$. The dimensionless reference temperature is set as $T_0 = 0.09$ (see Appendix A.2 for the expressions in corresponding dimensionless units). Note that in distinct contrast to Fig. 3(d) the ratchet effect now yields with a modulation strength $A \neq 0$ a nonvanishing heat flow at zero bias $\Delta = 0$. Applying a substantial rocking strength $A = 0.5$, the current bias characteristics can be manipulated to inhibit a negative differential thermal resistance (NDTR) regime at negative bias values Δ. Adapted from Li, Hänggi, and Li, 2008.

response frequency of the system, the intriguing phenomenon of a heat current *reversal* can be observed (Li, Hänggi, and Li, 2008; Li *et al.*, 2009). For this two-segment system, an optimal heat current can be obtained around this characteristic frequency even when the two isothermal baths are oscillating in synchrony with $T_L(t) = T_R(t)$, and the current reversal can be realized by tuning the system size (Ren and Li, 2010). In the harmonic mixing mechanism the directed heat current is found to be proportional to the third-order moment $\overline{[\Delta T(t)/2T_0]^3}$, i.e., $J \propto A_1^2 A_2 \cos\varphi$ (Li *et al.*, 2009). This enables a more efficient way of manipulating heat: the direction of the heat current can be reversed by merely adjusting the relative phase shift φ of the second-harmonic driving.

Apart from using the FK lattice as a source of nonlinearity, other schemes of heat motors are based on a FPU lattice structure, a Lennard-Jones interaction potential (Li *et al.*, 2009), or a Morse lattice structure (Gao and Zheng, 2011).

Besides a manipulation of bath temperatures, the shuttling of heat can be realized by use of a combination of time-dependent mechanical controls in otherwise symmetrical structures. Depending on specific nonlinear system setups, an emerging directed heat current can be controlled by adjusting the relative phase of the acting drive forces (Marathe, Jayannavar, and Dhar, 2007) or the driving frequency (Ai, He, and Hu, 2010). Multiple resonance structures for the heat current versus the driving frequency of external forces can occur as well (Zhang, Ren, and Li, 2011). It can be further demonstrated that for strict harmonic systems, periodic-force driving fails to shuttle heat. Moreover, it has been shown that even for anharmonic lattice segments composed of an additional energy depot, it is not possible to pump heat from a cold reservoir to a hot reservoir by merely applying external forces (Marathe, Jayannavar, and Dhar, 2007; Zhang, Ren, and Li, 2011).

It is instructive to compare these setups with the Feynman ratchet-and-pawl device of a heat pump (Komatsu and Nakagawa, 2006; Van den Broeck and Kawai, 2006; van den Broek and Van den Broeck, 2008; Hänggi and Marchesoni, 2009). The latter is a consequence of Onsager's reciprocal relation in the linear response regime: if a thermal bias generates a mechanical output, then an applied force will direct a heat flow as a conjugate behavior. Therefore, conjugated processes can be utilized for heat control as well. Other well-known thermally conjugated processes are the Seebeck, Thomson, and Peltier effects in thermoelectrical devices, where the thermal bias induces electrical currents, or vice versa. Recently, such a nanoscale magnetic heat engine and pump has been investigated for a magnetomechanical system, which either operates as an engine via the application of a thermal bias to convert heat into useful work or acts as a cooler via application of magnetic fields or mechanical force fields to pump heat (Bauer *et al.*, 2010).

B. Quantum heat shuttling

The efficient shuttling of heat via a time-dependent modulation of bath temperatures can be extended into the quantum regime when tunneling and other quantum fluctuation effects come into play. In clear contrast to the realm of electron shuttling (Hänggi, Ratner, and Yaliraki, 2002; Joachim and Ratner, 2005; Remacle, Heath, and Levine, 2005; Galperin, Ratner, and Nitzan, 2007; Hänggi and Marchesoni, 2009), however, this aspect of shuttling quantum heat is presently still at an initial stage, although expected to undergo increasing future activity.

1. Molecular wire setup

In the following we consider one specific such case in some detail. Consider a setup with a typical molecular wire for which the heat transport is generally governed by both electrons and phonons. A schematic setup based on a stylized molecular wire is sketched in Fig. 13(a) (Zhan *et al.*, 2009). The single electronic level E_1 can be conveniently modulated by a gate voltage and ω_1 denotes the vibrational frequency for a single phonon mode. The lead temperatures $T_{L(R)}(t)$ undergo an adiabatically slow periodic modulation for both electron and phonon reservoirs. The latter is experimentally accessible by use of a heating and cooling circulator (Lee, Govorov, and Kotov, 2005). In an adiabatic driving regime, the asymptotic ballistic electron and phonon heat currents $J_Q^{\mathrm{el(ph)}}(t)$ can be calculated via the Landauer-like expressions (Segal, Nitzan, and Hänggi, 2003; Dubi and Di Ventra, 2011) i.e.,

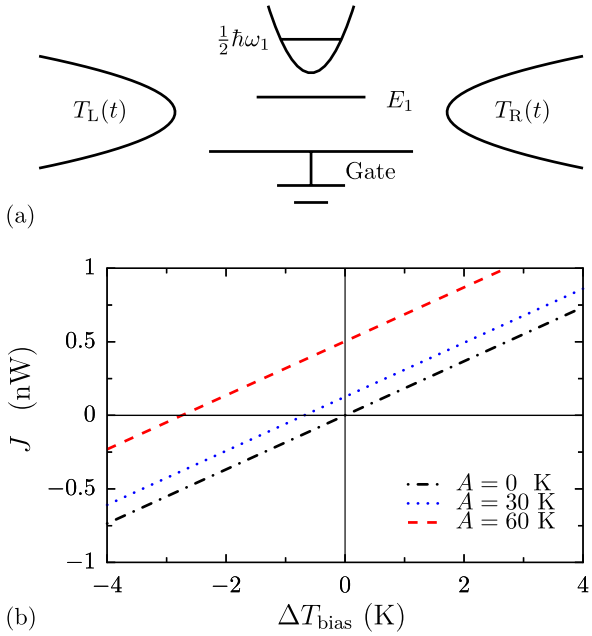

FIG. 13 (color online). Quantum heat shuttling. (a) Setup of a molecular junction acting as a heat shuttle. The short molecular wire is composed of a single electronic level E_1 only that can be gated and a single phonon mode at the fixed vibrational frequency $\omega_1 = 1.4 \times 10^{14}$ s^{-1}, typical for a carbon-carbon bond. The lead temperatures $T_{L(R)}(t)$ are subjected to time-periodic modulations. (b) Quantum thermal ratchet effect for this molecular junction. Total directed heat current J_Q as a function of static thermal bias ΔT_{bias} for different driving amplitude strengths A. The heat baths are modulated as $T_L(t) = T_0 + \frac{1}{2}\Delta T_{\mathrm{bias}} + A\cos\Omega t$ and $T_R(t) = T_0 - \frac{1}{2}\Delta T_{\mathrm{bias}}$. The reference temperature is set as $T_0 = 300$ K and the electronic wire level is set as $E_1 - \mu = 0.138$ eV, where μ is the chemical potential. J_Q is independent of the driving frequency Ω as a consequence of ballistic heat transfer in the adiabatic limit. From Zhan *et al.*, 2009.

$$J_Q^{\mathrm{el}}(t) = \int_{-\infty}^{\infty} \frac{d\varepsilon}{2\pi\hbar}(\varepsilon-\mu)\mathcal{T}^{\mathrm{el}}(\varepsilon)\{f[\varepsilon,T_L(t)]-f[\varepsilon,T_R(t)]\}, \tag{6}$$

$$J_Q^{\mathrm{ph}}(t) = \int_0^{\infty} \frac{d\omega}{2\pi}\hbar\omega\mathcal{T}^{\mathrm{ph}}(\omega)\{n[\omega,T_L(t)]-n[\omega,T_R(t)]\}, \tag{7}$$

where $\mathcal{T}^{\mathrm{el}}(\varepsilon)$ and $\mathcal{T}^{\mathrm{ph}}(\omega)$, respectively, denote the temperature-independent transmission probability for electrons with energy ε and phonons with angular frequency ω. Here the functions $f[\epsilon,T_l(t)]=\{\exp[(\epsilon-\mu_l)/k_{\mathrm{B}}T_l(t)]+1\}^{-1}$ and $n[\omega,T_l(t)]=\{\exp[\hbar\omega/k_{\mathrm{B}}T_l(t)]-1\}^{-1}$, where $l=L,R$ denote the Fermi-Dirac distribution and the Bose-Einstein distribution, respectively. These functions both inherit a time dependence which derives from the applied adiabatic periodic temperature modulation.

Then a finite total heat current J_Q emerges, reading

$$J_Q = \overline{J_Q^{\mathrm{el}}(t)+J_Q^{\mathrm{ph}}(t)}. \tag{8}$$

This heat current J_Q results as a consequence of the nonlinear dependence of quantum statistics on temperature [see Fig. 13(b)]; note that in the presence of modulation J_Q is nonzero even for vanishing thermal bias ΔT_{bias}. This ballistic heat transport is a pure quantum effect which will not occur in the classical diffusive limit, being approached at ultrahigh temperatures. The efficient manipulation of heat shuttling can be realized by applying the above-mentioned harmonic mixing mechanism. Since the heat transport is carried also by electrons, adjusting the gate voltage gives rise to an intriguing control of heat current with the result that the direction of the heat current experiences multiple reversals.

The quantum heat shuttling of a dielectric molecular wire can also be achieved by periodically modulating the molecular levels while this molecular wire is connected to two heat baths that are characterized by distinct spectral properties (Segal and Nitzan, 2006). Interestingly, the pumping of quantum heat can be operated arbitrarily close to the Carnot efficiency by a tailored stochastic modulation of the molecular levels (Segal, 2008, 2009). Time-dependent phonon transport in the nonadiabatic regime and strong driving perturbations have numerically been investigated by use of the nonequilibrium Green's function (NEGF) approach (Wang, Wang, and Lü, 2008; Dubi and Di Ventra, 2011) for the case of coupled harmonic oscillator chains: There, the coupling between the two reservoirs is switched on suddenly (Cuansing and Wang, 2010).

2. Pumping heat via geometrical phase

As discussed, a one-parameter modulation, e.g., via the left-sided contact temperature $T_L(t)$, is typically sufficient for quantum mechanical shuttling and rectification of heat, as shown in Fig. 14(a). It should be noted, however, that a cyclic modulation involving at least two control parameters generally induces additional current contributions beyond its mere dynamic component. This is so because with a variation evolving in a (parameter) space of dimension $d \geq 2$ one typically generates geometrical properties (i.e., a nonvanishing, gauge-invariant curvature) in the higher-dimensional

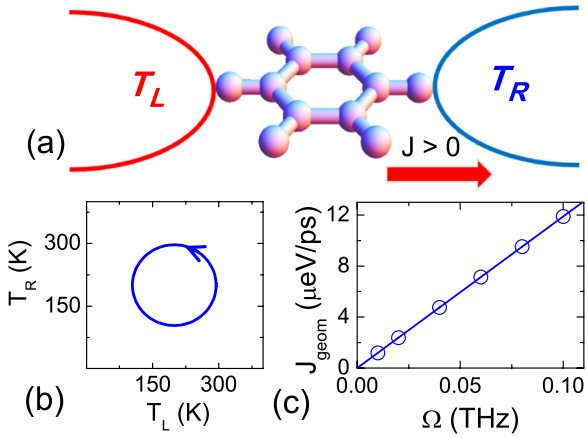

FIG. 14 (color online). Quantum heat pumping via a geometrical phase. (a) A schematic representation of a single molecular junction. (b) Quantum heat transfer across the molecular junction is generated via an adiabatic two-parameter variation of the left bath temperature $T_L(t)$ and the right bath temperature $T_R(t)$, which maps onto a closed circle. The arrow indicates the direction of the modulation protocol. (c) Geometrical-phase-induced heat current J_{geom} vs the angular modulation frequency Ω. The straight line corresponds to the analytic result while the open circles denote the simulation results. For further details see Ren *et al.*, 2010.

parameter space of the governing dynamical laws for the observable, in this case the heat flow. These geometrical properties in turn affect the resulting flow within an adiabatic or even nonadiabatic parameter variation. With a cyclic adiabatic variation of multiple parameters, this contribution to the emerging flow is thus of topological origin. It has been popularized in the literature under the label of a geometrical, finite-curvature, or (Berry) phase phenomenon (Sinitsyn, 2009). As a consequence, one needs to consider the total heat flow as composed of two contributions, reading

$$J_{\mathrm{tot}} = J_{\mathrm{dyn}} + J_{\mathrm{geom}}. \tag{9}$$

Here the geometrical contribution is proportional to the adiabatic small modulation frequency Ω, implying that this correction is typically quite small in comparison with the nonvanishing dynamical contribution. Therefore, to observe this component it is advantageous to use a two-parameter variation such that the dynamic component vanishes identically.

A solely geometrical contribution can be implemented, for example, by modulating the two bath temperatures in such a way that the trajectory in the plane spanned by the two temperatures describes a circle [see Fig. 14(b)] in which case there results a solely Berry-phase-induced heat current J_{geom}, while its dynamical component J_{dyn} is identically vanishing $J_{\mathrm{dyn}}=0$ (Ren, Hänggi, and Li, 2010). Also unlike the case of an irreversible, dynamical heat flux, this geometrical contribution can be reversed by simply reversing the protocol evolution. The latter operation thus provides a novel and convenient method for controlling energy transport. Ren, Hänggi, and Li (2010) demonstrated such nonvanishing quantum heat pumping as the result of a nonvanishing geometrical phase. This is shown in Fig. 14(c).

A similar geometrical phase effect can also be present in classical setups, e.g., for coupled harmonic oscillators in

contact with Langevin heat baths (Ren, Liu, and Li, 2012). In this case it was demonstrated that with a modulation of the two bath temperatures in time the geometrical phase phenomenon emerges only for the higher-order moments of the heat flow, that is to say, only beyond the average heat flux. Only when nonlinearity or temperature-dependent parameters in an interacting system are present can the geometrical phase manifest itself in producing a nonvanishing heat current. An electric circuitry experiment was also proposed to validate the above predictions (Ren, Liu, and Li, 2012).

Moreover, the finite Berry-phase heat pump mechanism in both quantum and classical systems was demonstrated to cause a breakdown of the "heat-flux fluctuation theorem," the latter being valid for a time-independent heat-flux transfer. This fluctuation theorem (Saito and Dhar, 2007; Campisi, Hänggi, and Talkner, 2011) can be restored only under special conditions in the presence of a vanishing Berry curvature (Ren, Hänggi, and Li, 2010).

C. Topological phonon Hall effect

It is known that a geometrical Berry phase has profound effects on electronic transport properties in various Hall effect setups (Xiao, Chang, and Niu, 2010). Because of the very different nature of electrons and phonons, the phonon Hall effect (PHE) was discovered only recently in a paramagnetic dielectric (Strohm, Rikken, and Wyder, 2005), and subsequently confirmed by yet a different experimental setup (Inyushkin and Taldenkov, 2007). In particular, one observes a transverse heat current in the direction perpendicular to the applied magnetic field and to the longitudinal temperature gradient; see Fig. 15. The discovery of this novel PHE renders the magnetic field as another flexible degree of freedom for phonon manipulation toward the objective of energy and information control in phononics.

Since then, several theoretical explanations have been proposed (Sheng, Sheng, and Ting, 2006; Kagan and Maksimov, 2008; Wang, and Zhang, 2009; Zhang, Wang, and Li, 2009) to understand the PHE by considering the spin-phonon coupling. This has two possible origins: Either (i) it derives from the magnetic vector potential in ionic crystal lattices, where the vibration of atoms with effective charges will experience the Lorentz force under magnetic fields (Holz, 1972), or (ii) it results from a Raman (spin-orbit) interaction (Kronig, 1939; Van Vleck, 1940; Orbach, 1961; Ioselevich and Capellmann, 1995). It has been shown that, by introducing spin-phonon couplings, a ballistic system without nonlinear interaction even exhibits the possibility of thermal rectification (Zhang, Wang, and Li, 2010).

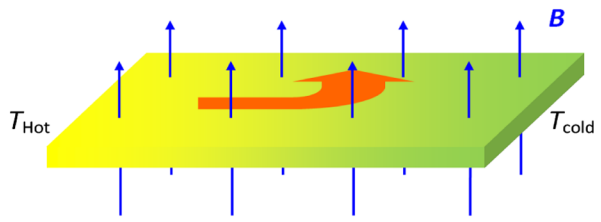

FIG. 15 (color online). A schematic illustration of the phonon Hall effect with heat flowing along the direction indicated by the large arrow.

Similar to that for the various Hall effects occurring for electrons, a topological explanation of the PHE was provided by Zhang, Wang, and Li (2010) and L. Zhang *et al.* (2011). The heat flow in the PHE is ascribed to two separate contributions: the normal flow responsible for the longitudinal phonon transport, and the anomalous flow manifesting itself as the Hall effect of the transverse phonon transport. A general expression for the transverse phonon Hall conductivity is obtained in terms of the Berry curvature of phononic band structures. The associated topological Chern number (a quantized integer) for each phonon band is defined via integrating the Berry curvature over the first Brillouin zone. For the two-dimensional honeycomb and kagome lattice, they observed phase transitions in the PHE, which correspond to the sudden change of the underlying band topology. The physical mechanism is rooted in the touching and splitting of the phonon bands (Zhang *et al.*, 2010; L. Zhang *et al.*, 2011).

Therefore, similar to electrons in topological insulators (Hasan and Kane, 2010), the design of a family of novel phononic devices, topological thermal insulators, is promising, with the bulk being an ordinary thermal insulator while the edge or surface constitutes an extraordinary thermal conductor.

V. SUMMARY, SUNDRIES, AND OUTLOOK

In this Colloquium we took the reader on a tour presenting the state of the art of the topic termed "phononics," an emerging research direction which is expected to be analogous in the future with conventional "electronics." In particular, we surveyed and explained various physical mechanisms that are exploited in devising the elementary tool kit: namely, a thermal diode or rectifier, a thermal transistor, a thermal logic gate, and thermal memory. These building blocks for phononic circuits are rooted in the application of suitable static or dynamic control schemes for shuttling heat. We further reviewed recent attempts to realize such phononic devices, which are all based on nanostructures, and discussed first experimental realizations.

A. Challenges

In spite of the rapid developments of phononics in both science and technology, we stress that this field is still at its outset. To put these phononic devices to work, there remain many difficult theoretical and severe experimental challenges to be overcome. For example, much work is still required on the physical realization of the phononic toolbox and to enter the next stage of assembling operating networks that are both scalable and stable under ambient conditions.

Theory.—Interface thermal resistance. As pointed out the underlying mechanism for a thermal rectifier or diode is based on an asymmetric interface thermal resistance. However, thus far a truly comprehensive theory for this effect is lacking.

The current approaches for thermal transport across an interface, such as the acoustic mismatch theory (Little, 1959) and the diffusive mismatch theory (Swartz and Pohl, 1989), are based on the assumption that phonon transport

proceeds via a combination of either ballistic or diffusive transport on either side of the interface. Both schemes offer limited accuracy for nanoscale interfacial resistance predictions (Stevens, Smith, and Norris, 2005), due to the neglect of the atomic details of actual interfaces. Specifically, the acoustic mismatch model assumes that phonons are transported across the interface without being scattered; i.e., they are ballistic, while the diffuse mismatch model assumes the opposite, namely, that the phonons are scattered diffusively. Thus, the effects of scattering on the interfacial thermal resistance act as upper and lower limits for a real situation. In fact, both numerical and experimental studies in nanostructures ranging from nanotubes (Zhang and Li, 2005; Chang *et al.*, 2008) and nanowires (Yang, Zhang, and Li, 2010) to polyethylene nanofibers (Henry and Chen, 2008, 2009; Shen *et al.*, 2010) all show that phonons undergo anomalous diffusion, i.e., superdiffusion, which is faster than normal diffusion but slower than ballistic transport. Therefore, it is necessary to establish an improved theory describing thermal transport across the interface by taking into account the anomalous thermal transport characteristics of nanostructures.

Yet another fact of thermal rectification and negative differential thermal resistance is the role of (strong) nonlinearity. To set up a transport theory by incorporating nonlinearity in both the quantum regime and the classical regime presents a challenge. The NEGF method (Wang, Wang, and Lü, 2008) certainly serves as an elegant mathematical framework. However, when sophisticated phonon-phonon interactions (which derive from anharmonicity) and the like become increasingly important (this being the case in realistic nanostructures), the NEGF presents a cumbersome task. In the classical regime, an effective phonon theory was proven useful in characterizing heat conduction (Li, Tong, and Li, 2006; Li and Li, 2007). Several classical studies have been advanced (He, Buyukdagli, and Hu, 2008, 2009; He *et al.*, 2010), which may also be extended into the quantum regime.

Experiment.—Experimental realization of a practical phononic device depends on how to measure its thermal conductivity accurately. To this end, one needs to get rid of the contact thermal resistance. Thus far no well-defined scheme capable of eradicating such contact thermal resistance has been put forward.

It also should be noted that presently the prime elementary phononic building block, i.e., the thermal rectifier, has been realized on the micrometer scale (Chang *et al.*, 2006) and on the millimeter scale (Kobayashi, Teraoka, and Terasaki, 2009; Sawaki *et al.*, 2011) only. The challenge for experimentalists is to make the sample smaller, for example, tens of nanometers or even a few nanometers only. This then would boost the rectification to much larger values and simultaneously would allow detection of the asymmetric interface thermal resistance. The primary challenge ahead, however, is to validate the negative differential thermal resistance, i.e., the key element necessary in realizing the thermal transistor.

For an electroniclike function networking toward a phononiclike logic operation is indispensable. In the event that this task could be achieved successfully it would then facilitate the desirable operation of an all-phononic computer.

B. Future prospects

As emphasized, the area of phononics is still in its infancy, but it is at the verge of blossoming.

From phononics to acoustics, and vice versa.—As elucidated throughout this Colloquium, the physical principle of phononic devices rests in the manipulation of phonon bands or spectra. This idea can be generalized to control any elastic or mechanical energy. For example, inspired by the thermal diode, an acoustic diode was proposed by Liang, Yuan, and Cheng (2009) and subsequently realized experimentally by use of a nonlinear acoustic medium and phononic crystal (Liang *et al.*, 2010) and a sonic crystal geometry (Li, *et al.*, 2011). Boechler, Theocharis, and Daraio (2011) demonstrated experimentally elastic energy switching and rectification. There is little doubt that, in parallel to phononics, an acoustic transistor, logic gate, and possibly even a computer device may be realized in the foreseeable future. The ideas and concepts in controlling acoustic waves can as well be exploited for phononics. For example, phononic crystals have been demonstrated to be useful in manipulating acoustic wave propagation (Liu *et al.*, 2000). This concept was extended recently to control heat flow on the nanoscale (McGaughey *et al.*, 2006; Landry, Hussein, and McGaughey, 2008; Yu *et al.*, 2010; Hopkins *et al.*, 2011). It would not come as too big of a surprise if some day concepts such as a "heat cloak," "super heat lens," etc., are realized via the implementation of phononic concepts by use of acoustic metamaterials (Yang *et al.*, 2004; Zhang and Liu, 2004; Fang *et al.*, 2006; Guenneau, Pétursson, and Ramakrishna, 2007). In fact, there is presently active research in controlling and manipulating elastic or mechanical energy ranging from long-wavelength elastic waves to very short-wavelength thermal waves; a glimpse of this activity can be found in El-Kady and Hussein (2011).

Phoxonics: phononics plus photonics, and beyond.—Another promising prospect is based on the combination of phononics with photonics to control and manage photon and phonon energy concomitantly (Maldovan and Thomas, 2006). This synergy might potentially enable one to use solar energy more wisely. For instance, a single-molecule phonon field-effect transistor was designed wherein phonon conductance is controlled by a back-gate electric field (Menezes *et al.*, 2010). Moreover, as temperature is the commonly applied control parameter for chemical and biological reactions, phononic devices may also find application for the local control of temperatures, for example, in regulating molecular self-assembling processes with the "lab-on-a-chip" technology.

Phononics and electronics.—Electrons carry heat as well. Therefore one can control the heat flow carried by electrons with the help of electric or magnetic fields. For example, by asymmetrically coupling a quantum dot to its two leads one can construct a heat rectifier (Scheibner, *et al.*, 2008); upon applying a gate voltage it is possible to operate a heat transistor (Saira, *et al.*, 2007). These kinds of devices combined with phononic circuits may then carry the potential to manipulate dissipation of heat and cooling in nanoscale and molecular devices. Overall, there is also the possibility that hybrid structures composed of electronic and phononic elements may lead to beneficial applications.

From heat conduction to radiation.—In this Colloquium, our proposed phononic devices are based on the control of heat conduction, assisted by lattice vibrations. A similar idea can be generalized to control heat radiation. Indeed, Fan and collaborators at Stanford proposed a photon-mediated "thermal rectifier through vacuum" (Otey, Lau, and Fan, 2010) which makes constructive use of the temperature dependence of underlying electromagnetic resonances. In the same spirit, Fan's group (Zhu, Otey, and Fan, 2012) revealed negative differential thermal conductance through vacuum; this in turn allows for the blueprint of a transistor for heat radiation.

Finally, we end with a celebrated quote by Winston Churchill: "This is not the end. It is not even the beginning of the end. But it is, perhaps, the end of the beginning."

ACKNOWLEDGMENTS

We thank G. Casati for most insightful discussions and fruitful collaborations during the early stages of this endeavor. We are also indebted to M. Peyrard for many useful discussions and valuable suggestions on this topic. Moreover, we are grateful to Bambi Hu, Pawel Keblinski, Zonghua Liu, Tomaz Prozen, Peiqing Tong, Jian-Sheng Wang, Jiao Wang, Changqin Wu, Hong Zhao, and our group members at NUS, Jie Chen, Jingwu Jiang, Jinghua Lan, Lihong Liang, Wei Chung Lo, Xin Lu, Xiaoxi Ni, Lihong Shi, Bui Cong Tinh, Ziqian Wang, Gang Wu, Rongguo Xie, Xiangfan Xu, Nuo Yang, Donglai Yao, Yong-Hong Yan, Lifa Zhang, Sha Liu, Dan Liu, Xiang-ming Zhao, Kai-Wen Zhang, Guimei Zhu, Jiayi Wang, and John T. L. Thong, for fruitful collaborations in different stages of this project. We also thank J. D. Bodyfelt for carefully reading parts of the manuscript and helpful comments. This work has been supported by grants from the Ministry of Education, Singapore, the Science and Engineering Research Council, Singapore, the National University of Singapore, and the Asian Office of Aerospace R&D (AOARD) of the U.S. Air Force by Grants No. R-144-000-285-646, No. R-144-000-280-305, and No. R-144-000-289-597, respectively; the startup fund from Tongji University (N. L. and B. L.), the National Natural Science Foundation of China, Grant No. 10874243 (L. W.), the Ministry of Science and Technology of China, Grant No. 2011CB933001, Ministry of Education, China, Grant No. 20110001120133 (G. Z.), by the German Excellence Initiative via the "Nanosystems Initiative Munich" (NIM) (P. H.), and also by the DFG Priority Program No. DFG-1243 "Quantum transport at the molecular scale" (P. H.).

APPENDIX: NONLINEAR LATTICE MODELS

1. Lattice models

In this Appendix we introduce three archetypical one-dimensional (1D) lattice models commonly used in the investigation of heat transport. These are (i) the linear harmonic lattice, (ii) the nonlinear Fermi-Pasta-Ulam β (FPU-β) lattice, and (iii) the Frenkel-Kontorova (FK) lattice. The simplest harmonic lattice serves as the basic model from which the FPU-β lattice and FK lattice are derived by complementing the dynamics with a nonlinear interatom interaction in the FPU case and an on-site potential in the FK case.

For a 1D harmonic lattice with N atoms the normal modes of the lattice vibrations are known as phonons. The corresponding harmonic lattice Hamiltonian explicitly reads

$$H = \sum_{i=1}^{N}\left[\frac{p_i^2}{2m} + \frac{k_0}{2}(x_i - x_{i-1} - a)^2\right], \tag{A1}$$

wherein the dynamical variables p_i and x_i, $i = 1, \ldots, N$ denote the momentum and position degrees of freedom for the ith atom and $x_0 \equiv x_1 - a$. The parameters m, k_0, and a denote the mass of the atom, the spring constant, and the lattice constant, respectively. The position variable x_i can be replaced by the displacement from equilibrium position as $\delta x_i = x_i - ia$ which we denote by the same symbol $x_i \equiv \delta x_i$ henceforth. The Hamiltonian of Eq. (A1) with $\delta x_0 = \delta x_1$ is thus simplified, reading

$$H = \sum_{i=1}^{N}\left[\frac{p_i^2}{2m} + \frac{k_0}{2}(x_i - x_{i-1})^2\right]. \tag{A2}$$

This form explicitly depicts the translational invariance of the free chain, which implies momentum conservation.

Applying next periodic boundary conditions $x_0 \equiv x_N$, the harmonic lattice of Eq. (A2) can be decomposed into the sum of noninteracting normal modes (phonons) with the dispersion relation reading

$$\omega(q) = 2\sqrt{\frac{k_0}{m}}|\sin(q/2)|, \qquad 0 \le q \le 2\pi, \tag{A3}$$

where the continuous spectrum is due to the adoption of the thermodynamical limit $N \to \infty$. The harmonic lattice possesses an acoustic phonon branch with $\omega(q) \to 0$ as $q \to 0$.

Although the 3D harmonic lattice model yields a satisfactory explanation for the temperature dependence of the experimentally measured specific heat, it turns out that this model of noninteracting phonon modes fails to describe a Fourier law for heat transport. In pioneering work, Rieder, Lebowitz, and Lieb (1967) proved that for this 1D harmonic lattice the heat transport is ballistic; this is due to the absence of phonon-phonon interactions. In order to take the phonon-phonon interactions into account, the harmonic chain model must be complemented with nonlinearity.

If a quartic interatom potential is added, one arrives at the FPU-β lattice with the corresponding Hamiltonian reading

$$H = \sum_{i=1}^{N}\left[\frac{p_i^2}{2m} + \frac{k_0}{2}(x_i - x_{i-1})^2 + \frac{\beta_0}{4}(x_i - x_{i-1})^4\right], \tag{A4}$$

where the parameter β_0 is the nonlinear coupling strength. Historically, the FPU-β lattice was put forward by Fermi, Pasta, and Ulam (1955) to study the issue of ergodicity of dynamics of a nonlinear system. For reviews of the original FPU problem see Ford (1992) and Berman and Izrailev (2005). Surprisingly, the FPU-β lattice still fails to obey Fourier's law and the heat conductivity κ diverges with the system size as $\kappa \propto N^{\alpha}$ with $0 < \alpha < 1$ (Lepri, Livi, and Politi, 1997). This divergent behavior was recently experimentally verified for a system setup using quasi-1D nanotubes (Chang *et al.*, 2008). The phonon modes of the FPU-β lattice are also acousticlike after renormalization of the nonlinear part, due to the conservation of total momentum.

If a periodic on-site substrate potential is added to the harmonic chain, one arrives at the FK lattice. Its Hamiltonian is given by

$$H=\sum_{i=1}^{N}\left[\frac{p_i^2}{2m}+\frac{k_0}{2}(x_i-x_{i-1})^2+\frac{V_0}{4\pi^2}\left(1-\cos\frac{2\pi x_i}{a}\right)\right], \tag{A5}$$

where the parameter $V_0/4\pi^2$ denotes the nonlinear on-site coupling strength. Here we consider only the commensurate case where the on-site potential assumes the same spatial periodicity as the harmonic lattice. Notably, this model with an on-site potential now breaks momentum conservation. Among the various phenomenological models that mimic solid-state systems, the FK model has been shown to provide a suitable theoretical description for possible nonlinear phenomena such as the occurrence of commensurate-incommensurate phase transitions (Floria and Mazo, 1996) and kinklike structures and the like (Braun and Kivshar, 1998, 2004). It has attracted interest since it was first proposed by Frenkel and Kontorova (1938, 1939) in order to study various surface phenomena. Recently it was established that the FK lattice indeed does exhibit normal heat conduction and thus obeys the Fourier law (Hu, Li, and Zhao, 1998). This normal behavior is attributed to the optical phonon mode, which opens a gap as the momentum conservation is broken with the on-site potential.

2. Local temperature and heat flow

Dimensionless units constitute practical tools for theoretical analysis and numerical simulations. Here we provide a brief introduction to the dimensionless units used in this Colloquium for the various lattice model setups.

We start with the simplest lattice model of the 1D harmonic lattice of Eq. (A2). For the harmonic lattice contacting a heat bath specified by a temperature T, there are four independent parameters m, a, k_0, and k_B, where k_B denotes the Boltzmann constant. The dimensions of all the physical quantities that typically enter the issue of heat transport can be expressed by the proper combination of these four independent parameters because there are only four fundamental physical units involved: length, time, mass, and temperature.

As a result, one can introduce the dimensionless variables by measuring lengths in units of $[a]$, momenta in units of $[a(mk_0)^{1/2}]$, temperature in units of $[k_0a^2/k_B]$, frequencies in units of $[(k_0/m)^{1/2}]$, energies in units of $[k_0a^2]$, and heat currents in units of $[a^2k_0^{3/2}/(2\pi m^{1/2})]$. In particular, the Hamiltonian of Eq. (A2) can be transformed into a dimensionless form if we implement the following substitutions:

$$H\rightarrow H[k_0a^2],\qquad p_i\rightarrow p_i[a(mk_0)^{1/2}],\qquad x_i\rightarrow x_i[a], \tag{A6}$$

where the transformed dynamical variables yield the dimensionless variables, giving

$$H=\sum_{i=1}^{N}\left[\frac{p_i^2}{2}+\frac{1}{2}(x_i-x_{i-1})^2\right]. \tag{A7}$$

Typical physical values for atom chains are as follows: $a\sim10^{-10}$ m, $\omega_0\sim10^{13}$ s^{-1}, $m\sim10^{-26}$–10^{-27} kg, and $k_B=1.38\times10^{-23}$ J K^{-1}; we have $[k_0a^2/k_B]\sim10^2$–10^3 K. This in turn implies that room temperature corresponds to a dimensionless temperature T of the order of 0.1–1 (Hu, Li, and Zhao, 1998).

To obtain the dimensionless FPU-β lattice from Eq. (A4), one cannot scale the five parameters $k_B=a=m=k_0=\beta_0=1$ because one of them is redundant. Applying the substitutions of Eq. (A6), we obtain the dimensionless form for the FPU-β Hamiltonian:

$$H=\sum_{i=1}^{N}\left[\frac{p_i^2}{2}+\frac{1}{2}(x_i-x_{i-1})^2+\frac{\beta}{4}(x_i-x_{i-1})^4\right], \tag{A8}$$

with the dimensionless parameter $\beta\equiv\beta_0a^2/k_0$. It is evident that the dimensionless nonlinear coupling strength β is generally not equal to unity. However, it can be shown that adjusting β becomes equivalent to varying the system energy or its temperature.

The dimensionless FK Hamiltonian can also be obtained by use of Eq. (A6):

$$H=\sum_{i=1}^{N}\left[\frac{p_i^2}{2}+\frac{1}{2}(x_i-x_{i-1})^2+\frac{V}{4\pi^2}[1-\cos(2\pi x_i)]\right], \tag{A9}$$

where the dimensionless on-site coupling strength $V\equiv V_0/k_0a^2$.

Thus far, we have dealt with homogeneous lattice Hamiltonians. For thermal devices with more than one segment, each segment may possess its own set of parameters, such as a different spring constant or nonlinear coupling strength. In those cases, the reference parameter, for instance k_0, used to define a transformation in Eq. (A6) may be chosen to correspond to a natural parameter of the corresponding segment. In particular, the dimensionless Hamiltonian for each individual segment of a coupled FK-FK lattice may be written as

$$H=\sum_{i=1}^{N}\left[\frac{p_i^2}{2}+\frac{k}{2}(x_i-x_{i-1})^2+\frac{V}{4\pi^2}[1-\cos(2\pi x_i)]\right], \tag{A10}$$

where k is measured with the reference to a parameter k_0 which is introduced *a priori*.

Next we discuss the results for expressing temperature and heat current in dimensionless units. In our classical simulations we typically used Langevin thermostats with coupling of the "contact" or end particles to the heat baths at their corresponding temperature. More precisely, one adds to the corresponding Newtonian equation of motion a Langevin fluctuating term which satisfies the fluctuation-dissipation relation; see, e.g., Hänggi, Talkner, and Borkovec (1990). Toward this goal we made use of the equipartition theorem of classical statistical mechanics to define, for example, the local temperature T_i via its average atomic kinetic energy, i.e.,

$$k_BT_i\equiv\left\langle\frac{p_i^2}{m}\right\rangle\rightarrow T_i\equiv\langle p_i^2\rangle, \tag{A11}$$

where the arrow indicates the dimensionless substitution $T_i\rightarrow T_i[k_0a^2/k_B]$ and $p_i\rightarrow p_i[a(mk_0)^{1/2}]$, and $\langle\cdots\rangle$ denotes the (long) time average or, equivalently, the ensemble average in numerical simulations, thus implicitly assuming ergodicity (in mean value).

Unlike that for temperature, the expression for the heat current is model dependent. To arrive at a compact expression

we first rewrite the 1D lattice Hamiltonian in the more general form

$$H = \sum_i \left[\frac{p_i^2}{2} + V(x_{i-1}, x_i) + U(x_i) \right], \tag{A12}$$

where $V(x_{i-1}, x_i)$ denotes the interatom potential and $U(x_i)$ is the on-site potential. As a result of the continuity equation for local energy, the local, momentary heat current can be expressed as (Lepri, Livi, and Politi, 2003)

$$J_i = -\dot{x}_i \frac{\partial V(x_{i-1}, x_i)}{\partial x_i}. \tag{A13}$$

Consequently, the expression for the heat current depends only on the form of the interatom potential $V(x_{i-1}, x_i)$. One should note that although the on-site potential $U(x_i)$ does not enter into the expression for the heat current explicitly, it does, however, influence the heat current implicitly through the dynamical equations of motion.

The heat currents themselves are again obtained via the time average over an extended time span. For steady-state setups with fixed bath temperatures the resulting heat currents are time independent and, as well, independent of the particular site index (i) within the particular chain segment. Likewise, with periodically varying bath temperatures $T(t)$, the resulting ensemble average is also time periodic; an additional time average over the temporal period of $T(t)$ yields the cycle-averaged, time-independent heat flux. Alternatively, an explicit long-time average again produces this very time-independent value for the heat current.

3. Power spectra of FPU-β and FK lattices

The power spectrum (or power spectral density) describes the distribution of a system's kinetic energy falling within given frequency intervals. For a homogeneous lattice composed of identical particles the velocity $v_i(t) \equiv v(t)$ of a particle located at site i becomes independent of position i; the power spectrum then can be conveniently calculated by the Fourier transform of the corresponding velocity degree of freedom to yield

$$P(\omega) = \left| \lim_{t_0 \to \infty} \frac{1}{t_0} \int_0^{t_0} v(t) e^{-i\omega t} dt \right|^2. \tag{A14}$$

The power spectrum of the FPU-β model of Eq. (A8) depends on the temperature. In the low-temperature regime the FPU-β dynamics is close to that of a harmonic lattice, yielding $0 < \omega < 2$. In contrast, in the high-temperature regime it is the anharmonic part that starts to dominate. In this latter regime an approximate theoretical estimate then yields $0 < \omega < C_0(T\beta)^{1/4}$, with $C_0 = 2\sqrt{2\pi}\Gamma(3/4)3^{1/4}/\Gamma(1/4) \approx 2.23$, where Γ denotes the gamma function (Li, Lan, and Wang, 2005). Therefore, an increase in the temperature then causes a rightward shift of the power spectrum toward higher frequencies. Parseval's theorem then dictates that the area below the curve is proportional to the average kinetic energy of the particle, i.e., $\int_0^\infty P(\omega) d\omega \sim \langle E_{\rm kin} \rangle$.

For the FK model in Eq. (A10) the form of the power spectrum depends sensitively on temperature. In the low-temperature limit, the atoms are confined in the valley of the on-site potential. Upon linearizing Eq. (A10) the phonon band can be extracted to read

$$\sqrt{V} < \omega < \sqrt{V + 4k}. \tag{A15}$$

In contrast, in the high-temperature limit the on-site potential can be neglected; thus the system dynamics becomes effectively reduced to a harmonic chain dynamics, whose phonon band extends to

$$0 < \omega < 2\sqrt{k}. \tag{A16}$$

The crossover temperature T_c can be approximated as $T_{cr} \approx V/(2\pi)^2$. Its value depends on the height of the on-site potential. This in turn implies different values for the two segments of the thermal diode setup; see Fig. 16. This difference is at the heart of the thermal rectifying mechanism.

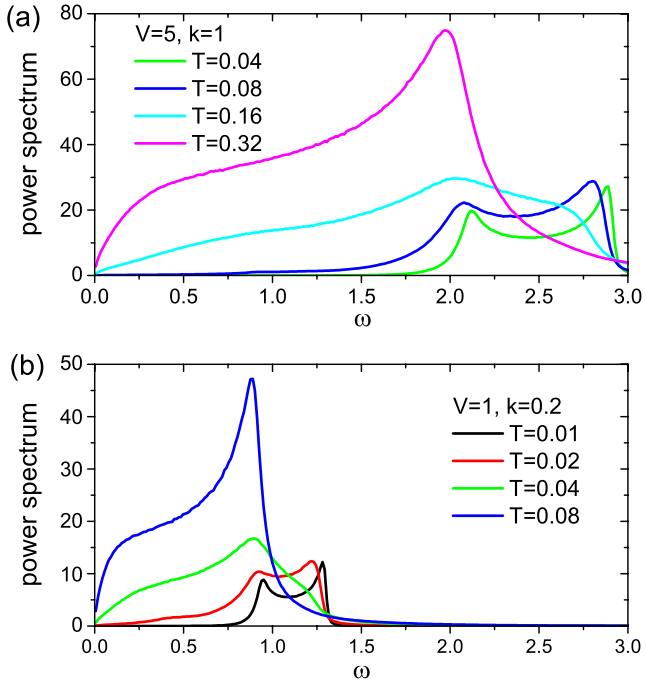

FIG. 16 (color online). Temperature-dependent power spectra. The variation of the power spectrum at different temperatures vs the angular frequency ω (both in dimensionless units) in a FK lattice with 10 000 sites for two different sets of parameters in (a) and (b). The features of these nonlinear FK power spectra provide the seed for the *modus operandi* in a thermal diode setup as discussed in Sec II.A.1. (a) FK coupling strength of $V = 5$ and a strength for the spring constant of $k = 1$; (b) coupling strength $V = 1$ and a spring constant value set at $k = 0.2$.

REFERENCES

Ai, B. Q., D. He, and B. Hu, 2010, "Heat conduction in driven Frenkel-Kontorova lattices: Thermal pumping and resonance," Phys. Rev. E **81**, 031124.

Astumian, R. D., and P. Hänggi, 2002, "Brownian motors," Phys. Today **55**, No. 11, 33.

Balandin, A. A., 2005, "Nanophononics: Phonon engineering in nanostructures and nanodevices," J. Nanosci. Nanotechnol. **5**, 1015.

Balandin, A. A., E. P. Pokatilov, and D. L. Nika, 2007, "Phonon engineering in hetero- and nanostructures," J. Nanoelectron. Optoelectron. **2**, 140.

Bardeen, J., and W. H. Brattain, 1948, "The Transistor, A Semi-Conductor Triode," Phys. Rev. **74**, 230.

Bauer, G. E. W., S. Bretzel, A. Brataas, and Y. Tserkovnyak, 2010, "Nanoscale magnetic heat pumps and engines," Phys. Rev. B **81**, 024427.

Berman, G. P., and F. M. Izrailev, 2005, "The Fermi-Pasta-Ulam problem: Fifty years of progress," Chaos **15**, 015104.

Boechler, N., G. Theocharis, and C. Daraio, 2011, "Bifurcation-based acoustic switching and rectification," Nature Mater. **10**, 665.

Braun, O. M., and Y. S. Kivshar, 1998, "Nonlinear dynamics of the Frenkel-Kontorova model," Phys. Rep. **306**, 1.

Braun, O. M., and Y. S. Kivshar, 2004, *The Frenkel-Kontorova Model: Concepts, Methods, and Applications* (Springer, Berlin).

Callen, H. B., 1960, *Thermodynamics: An Introduction to The Physical Theories of Equilibrium Thermostatics and Irreversible Thermodynamics* (Wiley, New York).

Campisi, M., P. Hänggi, and P. Talkner, 2011, "Quantum fluctuation relations: Foundations and applications," Rev. Mod. Phys. **83**, 771.

Casati, G., 2005, "Controlling the heat flow: Now it is possible," Chaos **15**, 015120.

Chang, C. W., D. Okawa, H. Garcia, A. Majumdar, and A. Zettl, 2007, "Nanotube Phonon Waveguide," Phys. Rev. Lett. **99**, 045901.

Chang, C. W., D. Okawa, H. Garcia, A. Majumdar, and A. Zettl, 2008, "Breakdown of Fourier's Law in Nanotube Thermal Conductors," Phys. Rev. Lett. **101**, 075903.

Chang, C. W., D. Okawa, A. Majumdar, and A. Zettl, 2006, "Solid-State Thermal Rectifier," Science **314**, 1121.

Chen, G., 2005, *Nanoscale Energy Transfer and Conversion* (Oxford University Press, New York).

Cuansing, E. C., and J.-S. Wang, 2010, "Transient behavior of heat transport in a thermal switch," Phys. Rev. B **81**, 052302.

Dhar, A., 2008, "Heat transport in low-dimensional systems," Adv. Phys. **57**, 457.

Dubi, Y., and M. Di Ventra, 2011, "Heat flow and thermoelectricity in atomic and molecular junctions," Rev. Mod. Phys. **83**, 131.

El-Kady, I., and M. I. Hussein, 2011, "Preface to Special Topic: Selected Articles from Phononics 2011: The First International Conference on Phononic Crystals, Metamaterials and Optomechanics, 29 May–2 June 2011, Santa Fe, New Mexico, USA," AIP Adv. **1**, 041301.

Esaki, L., 1958, "New Phenomenon in Narrow Germanium $p - n$ Junctions," Phys. Rev. **109**, 603.

Fang, N., D. Xi, J. Xu, M. Ambati, W. Srituravanich, C. Sun, and X. Zhang, 2006, "Ultrasonic metamaterials with negative modulus," Nature Mater. **5**, 452.

Fermi, E., J. Pasta, and S. Ulam, 1955, "Studies of the Nonlinear Problems, I," Los Alamos Report No. LA 1940.

Floria, L. M., and J. J. Mazo, 1996, "Dissipative dynamics of the Frenkel-Kontorova model," Adv. Phys. **45**, 505.

Ford, J., 1992, "The Fermi-Pasta-Ulam problem: Paradox turns discovery," Phys. Rep. **213**, 271.

Frenkel, J., and T. Kontorova, 1938, "On the theory of plastic deformation and twinning," Phys. Z. Sowiet Union **13**, 1.

Frenkel, J., and T. Kontorova, 1939, "On the theory of plastic deformation and twinning," J. Phys.-USSR **1**, 137.

Galperin, M., M. A. Ratner, and A. Nitzan, 2007, "Molecular Transport Junctions: Vibrational Effects," J. Phys. Condens. Matter **19**, 103201.

Gao, X.-Y., and Z.-G. Zheng, 2011, "Ratcheting thermal conduction in one-dimensional homogeneous Morse lattice systems," Acta Phys. Sin. **60**, 044401 [http://wulixb.iphy.ac.cn/EN/abstract/abstract18243.shtml].

Ghosh, S., W. Z. Bao, D. L. Nika, S. Subrina, E. P. Pokatliov, C. N. Lau, and A. A. Balandin, 2010, "Dimensional crossover of thermal transport in few-layer graphene," Nature Mater. **9**, 555.

Giazotto, F., T. T. Heikkilä, A. Luukanen, A. M. Savin, and J. P. Pekola, 2006, "Opportunities for mesoscopics in thermometry and refrigeration," Rev. Mod. Phys. **78**, 217.

Gonzalez Noya, E., D. Srivastava, and M. Menon, 2009, "Heat-pulse rectification in carbon nanotube Y junctions," Phys. Rev. B **79**, 115432.

Guenneau, S., A. M. G. Pétursson, and S. A. Ramakrishna, 2007, "Acoustic metamaterials for sound focusing and confinement," New J. Phys. **9**, 399.

Hänggi, P., and F. Marchesoni, 2009, "Artificial Brownian motors: Controlling transport on the nanoscale," Rev. Mod. Phys. **81**, 387.

Hänggi, P., F. Marchesoni, and F. Nori, 2005, "Brownian motors," Ann. Phys. (Berlin) **14**, 51.

Hänggi, P., M. Ratner, and S. Yaliraki, 2002, "Transport in molecular wires," Chem. Phys. **281**, 111.

Hänggi, P., P. Talkner, and M. Borkovec, 1990, "Reaction-rate theory: Fifty years after Kramers," Rev. Mod. Phys. **62**, 251.

Hasan, M. Z., and C. L. Kane, 2010, "Topological insultors," Rev. Mod. Phys. **82**, 3045.

He, D. H., B. Q. Ai, H. K. Chan, and B. Hu, 2010, "Heat conduction in the nonlinear response regime: Scaling, boundary jumps, and negative differential thermal resistance," Phys. Rev. E **81**, 041131.

He, D. H., S. Buyukdagli, and B. Hu, 2008, "Thermal conductivity of anharmonic lattices: Effective phonons and quantum corrections," Phys. Rev. E **78**, 061103.

He, D. H., S. Buyukdagli, and B. Hu, 2009, "Origin of negative differential thermal resistance in a chain of two weakly coupled nonlinear lattices," Phys. Rev. B **80**, 104302.

Henry, A., and G. Chen, 2008, "High Thermal Conductivity of Single Polyethylene Chains Using Molecular Dynamics Simulations," Phys. Rev. Lett. **101**, 235502.

Henry, A., and G. Chen, 2009, "Anomalous heat conduction in polyethylene chains: Theory and molecular dynamics simulations," Phys. Rev. B **79**, 144305.

Holz, A., 1972, "Phonons in a strong static magnetic field," Nuovo Cimento Soc. Ital. Fis. B **9**, 83.

Hopkins, P., C. M. Reinke, M. F. Su, R. H. Olsson, E. A. Shaner, Z. C. Leseman, J. R. Serrano, L. M. Phinney, and I. El-Kady, 2011, "Reduction in the thermal conductivity of single crystalline silicon by phononic crystal patterning," Nano Lett. **11**, 107.

Hu, B., D. He, L. Yang, and Y. Zhang, 2006, "Thermal Rectifying Effect in Macroscopic Size," Phys. Rev. E **74**, 060201.

Hu, B., B. Li, and H. Zhao, 1998, "Heat conduction in one-dimensional chains," Phys. Rev. E **57**, 2992.

Hu, J., X. Ruan, and Y. P. Chen, 2009, "Thermal Conductivity and Thermal Rectification in Graphene Nanoribbons: A Molecular Dynamics Study," Nano Lett. **9**, 2730.

Hu, M., P. Keblinski, and B. Li, 2008, "Thermal rectification at silicon-amorphous polyethylene interface," Appl. Phys. Lett. **92**, 211908.

Inyushkin, A. V., and A. N. Taldenkov, 2007, "On the phonon Hall effect in a paramagnetic dielectric," JETP Lett. **86**, 379.

Ioselevich, A. S., and H. Capellmann, 1995, "Strongly correlated spin-phonon systems: A scenario for heavy fermions," Phys. Rev. B **51**, 11 446.

Jiang, J., J. Wang, and B. Li, 2010, "Topology-induced thermal rectification in carbon nanodevices," Europhys. Lett. **89**, 46 005.

Joachim, C., and M. A. Ratner, 2005, "Molecular electronics: Some views on transport junctions and beyond," Proc. Natl. Acad. Sci. U.S.A. **102**, 8801.
Kagan, Y., and L. A. Maksimov, 2008, "Anomalous Hall Effect for the Phonon Heat Conductivity in Paramagnetic Dielectrics," Phys. Rev. Lett. **100**, 145902.
Kapitza, P. L., 1941, "The study of heat transfer in helium II," J. Phys. (USSR) **4**, 181.
Kim, P., L. Shi, A. Majumdar, and P. L. McEuen, 2001, "Thermal transport measurements of individual multiwalled nanotubes," Phys. Rev. Lett. **87**, 215502.
Kobayashi, W., Y. Teraoka, and I. Terasaki, 2009, "An oxide thermal rectifier," Appl. Phys. Lett. **95**, 171905.
Komatsu, T. S., and N. Ito, 2011, "Thermal transistor utilizing gas-liquid transition," Phys. Rev. E **83**, 012104.
Komatsu, T. S., and N. Nakagawa, 2006, "Hidden heat transfer in equilibrium states implies directed motion in nonequilibrium states," Phys. Rev. E **73**, 065107(R).
Kronig, R. d. L., 1939, "On the mechanism of paramagnetic relaxation," Physica (Amsterdam) **6**, 33.
Landry, E. S., M. I. Hussein, and A. J. H. McGaughey, 2008, "Complex superlattice unit cell designs for reduced thermal conductivity," Phys. Rev. B **77**, 184302.
Lee, J., A. O. Govorov, and N. A. Kotov, 2005, "Nanoparticle Assemblies with Molecular Springs: A Nanoscale Thermometer," Angew. Chem., Int. Ed. **44**, 7439.
Lepri, S., R. Livi, and A. Politi, 1997, "Heat Conduction in Chains of Nonlinear Oscillators," Phys. Rev. Lett. **78**, 1896.
Lepri, S., R. Livi, and A. Politi, 2003, "Thermal conduction in classical low-dimensional lattices," Phys. Rep. **377**, 1.
Li, B., J. H. Lan, and L. Wang, 2005, "Interface Thermal Resistance between Dissimilar Anharmonic Lattices," Phys. Rev. Lett. **95**, 104302.
Li, B., J. Wang, L. Wang, and G. Zhang, 2005, "Anomalous heat conduction and anomalous diffusion in nonlinear lattces, single wall nanotubes, and billiard gas channels," Chaos **15**, 015121.
Li, B., L. Wang, and G. Casati, 2004, "Thermal Diode: Rectification of Heat Flux," Phys. Rev. Lett. **93**, 184301.
Li, B., L. Wang, and G. Casati, 2006, "Negative differential resistance and thermal transistor," Appl. Phys. Lett. **88**, 143501.
Li, N., P. Hänggi, and B. Li, 2008, "Ratcheting heat flux against a thermal bias," Europhys. Lett. **84**, 40 009.
Li, N., and B. Li, 2007, "Temperature dependence of thermal conductivity in 1d nonlinear lattice," Europhys. Lett. **78**, 34 001.
Li, N., P. Q. Tong, and B. Li, 2006, "Effective phonons in anharmonic lattices: anomalous vs normal heat conduction," Europhys. Lett. **75**, 49.
Li, N., F. Zhan, P. Hänggi, and B. Li, 2009, "Shuttling heat across 1D homogenous nonlinear lattices with a Brownian heat motor," Phys. Rev. E **80**, 011125.
Li, W., H. Sevincli, G. Cuniberti, and S. Roche, 2010, "Phonon transport in large scale carbon-based disordered materials: Implementation of an efficient order-N and real-space Kubo methodology," Phys. Rev. B **82**, 041410.
Li, X.-F., X. Ni, L. Feng, M.-H. Lu, C. He, and Y.-F. Chen, 2011, "Tunable Unidirectional Sound Propagation through a Sonic-Crystal-Based Acoustic Diode," Phys. Rev. Lett. **106**, 084301.
Liang, B., X. Guo, J. Tu, D. Zhang, and J. Cheng, 2010, "An acoustic rectifier," Nature Mater. **9**, 989.
Liang, B., B. Yuan, and J.-c. Cheng, 2009, "Acoustic Diode: Rectification of Acoustic Energy Flux in One-Dimensional Systems," Phys. Rev. Lett. **103**, 104301.
Little, W. A., 1959, "The transport of heat between dissimilar solids at low temperatures," Can. J. Phys. **37**, 334.
Liu, Z., X. Zhang, Y. Mao, Y. Y. Zhu, Z. Yang, C. T. Chan, and P. Sheng, 2000, "Locally Resonant Sonic Materials," Science **289**, 1734.
Lo, W., L. Wang, and B. Li, 2008, "Thermal Transistor: Switching and Modulating Heat Flux," J. Phys. Soc. Jpn. **77**, 054402.
Maldovan, M., and E. L. Thomas, 2006, "Simultaneous localization of photons and phonons in two-dimensional periodic structures," Appl. Phys. Lett. **88**, 251907.
Marathe, R., A. M. Jayannavar, and A. Dhar, 2007, "Two simple models of classical heat pumps," Phys. Rev. E **75**, 030103(R).
McGaughey, A. J. H., M. I. Hussein, E. S. Landry, M. Kaviany, and G. M. Hulbert, 2006, "Phonon band structure and thermal transport correlation in a layered diatomic crystal," Phys. Rev. B **74**, 104304.
Menezes, M. G., A. Saraiva-Souza, J. Del Nero, and R. B. Capaz, 2010, "Proposal for a single-molecule field-effect transistor for phonons," Phys. Rev. B **81**, 012302.
Orbach, R., 1961, "Spin-Lattice Relaxation in Rare-Earth Salts," Proc. R. Soc. A **264**, 458.
Otey, C. R., W. T. Lau, and S. Fan, 2010, "Thermal Rectification through Vacuum," Phys. Rev. Lett. **104**, 154301.
Pollack, G. L., 1969, "Kapitza Resistance," Rev. Mod. Phys. **41**, 48.
Pop, E., 2010, "Energy Dissipation and Transport in Nanoscale Devices," Nano Res. **3**, 147.
Remacle, F., J. R. Heath, and R. D. Levine, 2005, "Electrical addressing of confined quantum systems for quasiclassical computation and finite state logic machines," Proc. Natl. Acad. Sci. U.S.A. **102**, 5653.
Ren, J., P. Hänggi, and B. Li, 2010, "Berry-phase induced heat pumping and its impact on the fluctuation theorem," Phys. Rev. Lett. **104**, 170601.
Ren, J., and B. Li, 2010, "Emergence and control of heat current from strict zero thermal bias," Phys. Rev. E **81**, 021111.
Ren, J., S. Liu, and B. Li, 2012, "Geometric Heat Flux for Classical Thermal Transport in Interacting Open Systems," Phys. Rev. Lett. **108**, 210603.
Rieder, Z., J. L. Lebowitz, and E. Lieb, 1967, "Properties of a Harmonic Crystal in a Stationary Nonequilibrium State," J. Math. Phys. (N.Y.) **8**, 1073.
Roberts, N. A., and D. G. Walker, 2011, "A review of thermal rectification observations and models in solid materials," Int. J. Therm. Sci. **50**, 648.
Saira, O.-P., M. Meschke, F. Giazotto, A. M. Savin, M. Möttönen, and J. P. Pekola, 2007, "Heat Transistor: Demonstration of Gate-Controlled Electronic Refrigeration," Phys. Rev. Lett. **99**, 027203.
Saito, K., and A. Dhar, 2007, "Fluctuation theorem in quantum heat conduction," Phys. Rev. Lett. **99**, 180601.
Saito, K., and A. Dhar, 2010, "Heat Conduction in a Three Dimensional Anharmonic Crystal," Phys. Rev. Lett. **104**, 040601.
Sawaki, D., W. Kobayashi, Y. Moritomo, and I. Terasaki, 2011, "Thermal rectification in bulk materials with asymmetric shape," Appl. Phys. Lett. **98**, 081915.
Scheibner, R., M. Konig, D. Reuter, A. D. Wieck, C. Gould, H. Buhmann, and L. W. Molenkamp, 2008, "Quantum dot as thermal rectifier," New J. Phys. **10**, 083016.
Segal, D., 2008, "Stochastic Pumping of Heat: Approaching the Carnot Efficiency," Phys. Rev. Lett. **101**, 260601.
Segal, D., 2009, "Vibrational relaxation in the Kubo oscillator: Stochastic pumping of heat," J. Chem. Phys. **130**, 134510.
Segal, D., and A. Nitzan, 2006, "Molecular heat pump," Phys. Rev. E **73**, 026109.
Segal, D., A. Nitzan, and P. Hänggi, 2003, "Thermal conductance through molecular wires," J. Chem. Phys. **119**, 6840.

Shao, Z. G., L. Yang, H. K. Chan, and B. Hu, 2009, "Transition from the exhibition to the nonexhibition of negative differential thermal resistance in the two-segment Frenkel-Kontorova model," Phys. Rev. E **79**, 061119.

Shen, S., A. Henry, J. Tong, R. Zheng, and G. Chen, 2010, "Polyethylene nanofibres with very high thermal conductivities," Nature Nanotech. **5**, 251.

Sheng, L., D. N. Sheng, and C. S. Ting, 2006, "Theory of the Phonon Hall Effect in Paramagnetic Dielectrics," Phys. Rev. Lett. **96**, 155901.

Sinitsyn, N. A., 2009, "The stochastic pump effect and geometric phases in dissipative and stochastic systems," J. Phys. A **42**, 193001.

Starr, C., 1936, "The Copper Oxide Rectifier," J. Appl. Phys. **7**, 15.

Stevens, R., A. Smith, and P. Norris, 2005, "Measurement of Thermal Boundary Conductance of a Series of Metal-Dielectric Interfaces by the Transient Thermoreflectance Technique," J. Heat Transfer **127**, 315.

Strohm, C., G. L. J. A. Rikken, and P. Wyder, 2005, "Phenomenological Evidence for the Phonon Hall Effect," Phys. Rev. Lett. **95**, 155901.

Swartz, E. T., and R. O. Pohl, 1989, "Thermal boundary resistance," Rev. Mod. Phys. **61**, 605.

Terraneo, M., M. Peyrard, and G. Casati, 2002, "Controlling the Energy Flow in Nonlinear Lattices: A Model for a Thermal Rectifier," Phys. Rev. Lett. **88**, 094302.

Van den Broeck, C., and R. Kawai, 2006, "Brownian Refrigerator," Phys. Rev. Lett. **96**, 210601.

van den Broek, M., and C. Van den Broeck, 2008, "Chiral Brownian Heat Pump," Phys. Rev. Lett. **100**, 130601.

Van Vleck, J. H., 1940, "Paramagnetic Relaxation Times for Titanium and Chrome Alum," Phys. Rev. **57**, 426.

Wang, L., and B. Li, 2007, "Thermal Logic Gates: Computation with Phonons," Phys. Rev. Lett. **99**, 177208.

Wang, L., and B. Li, 2008a, "Phononics gets hot," Phys. World **21**, 27 [http://physicsworldarchive.iop.org/index.cfm?action=summary&doc=21%2F03%2Fphwv21i03a31%40pwa-xml&qt=].

Wang, L., and B. Li, 2008b, "Thermal Memory: A Storage of Phononic Information," Phys. Rev. Lett. **101**, 267203.

Wang, J.-S., J. Wang, and J. T. Lü, 2008, "Quantum thermal transport in nanostructures," Eur. Phys. J. B **62**, 381.

Wang, J.-S., and L. Zhang, 2009, "Phonon Hall thermal conductivity from the Green-Kubo formula," Phys. Rev. B **80**, 012301.

Wu, G., and B. Li, 2007, "Thermal rectification in carbon nanotube intramolecular junctions: Molecular dynamics calculations," Phys. Rev. B **76**, 085424.

Wu, G., and B. Li, 2008, "Thermal rectifier from deformed carbon nanohorns," J. Phys. Condens. Matter **20**, 175211.

Wu, L. A., and D. Segal, 2009, "Sufficient Conditions for Thermal Rectification in Hybrid Quantum Structures," Phys. Rev. Lett. **102**, 095503.

Wu, L. A., C. X. Yu, and D. Segal, 2009, "Nonlinear quantum heat transfer in hybrid structures: Sufficient conditions for thermal rectification," Phys. Rev. E **80**, 041103.

Xiao, D., M.-C. Chang, and Q. Niu, 2010, "Berry phase effects on electronic properties," Rev. Mod. Phys. **82**, 1959.

Xie, R., C. T. Bui, B. Varghese, Q. Zhang, C. H. Sow, B. Li, and J. T. L. Thong, 2011, "An Electrically Tuned Solid-State Thermal Memory Based on Metal-Insulator Transition of Single-Crystalline VO2 Nanobeams," Adv. Funct. Mater. **21**, 1602.

Yang, N., N. Li, L. Wang, and B. Li, 2007, "Thermal rectification and negative differential thermal resistance in lattices with mass gradient," Phys. Rev. B **76**, 020301.

Yang, N., G. Zhang, and B. Li, 2008, "Carbon nanocone: A promising thermal rectifier," Appl. Phys. Lett. **93**, 243111.

Yang, N., G. Zhang, and B. Li, 2009, "Thermal Rectification In Asymmetric Graphene Ribbons," Appl. Phys. Lett. **95**, 033107.

Yang, N., G. Zhang, and B. Li, 2010, "Violation of Fourier's Law and Anomalous Heat Diffusion in Silicon Nanowires," Nano Today **5**, 85.

Yang, S., J. H. Page, Z. Liu, M. L. Cowan, C. T. Chan, and P. Sheng, 2004, "Focusing of Sound in a 3D Phononic Crystal," Phys. Rev. Lett. **93**, 024301.

Yu, J. K., S. Mitrovic, D. Tham, J. Varghese, and J. R. Heath, 2010, "Reduction of thermal conductivity in phononic nanomesh structures," Nat. Nanotechnol. **5**, 718.

Zhan, F., N. Li, S. Kohler, and P. Hänggi, 2009, "Molecular wires acting as quantum heat ratchets," Phys. Rev. E **80**, 061115.

Zhang, G., and B. Li, 2005, "Anomalous vibrational energy diffusion in carbon nanotubes," J. Chem. Phys. **123**, 014705.

Zhang, G., and B. Li, 2010, "Impacts of Doping On Thermal And Thermoelectric Properties of Nano Materials," Nanoscale **2**, 1058.

Zhang, G., and H. Zhang, 2011, "Thermal conduction and rectification in few-layer graphene Y Junctions," Nanoscale **3**, 4604.

Zhang, L., J.-S. Wang, and B. Li, 2010, "Ballistic thermal rectification in nanoscale three-terminal junctions," Phys. Rev. B **81**, 100301.

Zhang, L., J.-S. Wang, and B. Li, 2009, "Phonon Hall effect in four-terminal nano-junctions," New J. Phys. **11**, 113038.

Zhang, L., J. Ren, J.-S. Wang, and B. Li, 2010, "Topological Nature of Phonon Hall Effect," Phys. Rev. Lett. **105**, 225901.

Zhang, L., J. Ren, J.-S. Wang, and B. Li, 2011, "The phonon Hall effect: theory and application," J. Phys. Condens. Matter **23**, 305402.

Zhang, S., J. Ren, and B. Li, 2011, "Multiresonance of energy transport and absence of heat pump in a force-driven lattice," Phys. Rev. E **84**, 031122.

Zhang, X., and Z. Liu, 2004, "Negative refraction of acoustic waves in two-dimensional phononic crystals," Appl. Phys. Lett. **85**, 341.

Zhu, L. X., C. R. Otey, and S. Fan, 2012, "Negative Differential Thermal Conductance through Vacuum," Appl. Phys. Lett. **100**, 044104.

Zimen, J. M., 2001, *Electrons and Phonons: The Theory of Transport Phenomena in Solids* (Oxford University Press, New York).